# Enduring impacts of El Niño on life expectancy in past and future climates

**Authors:** Yanbin Xu[1]*, Wenjun Zhu[1], Dhrubajyoti Samanta[2], Benjamin P. Horton[3]*

**Affiliations:**

[1]Department of Banking and Finance, Nanyang Business School, Nanyang Technological University; Singapore.

[2]Earth Observatory of Singapore, Nanyang Technological University; Singapore.

[3]School of Energy and Environment, City University of Hong Kong; Hong Kong SAR.

*Corresponding author. Email: yanbin.xu@ntu.edu.sg, bphorton@cityu.edu.hk

*A revised version of this manuscript has been published in Nature Climate Change.*

*Final version: https://www.nature.com/articles/s41558-025-02534-4*

*DOI: 10.1038/s41558-025-02534-4*

**The El Niño–Southern Oscillation (ENSO) is a major driver of global climate variability, yet its long-term effect on life expectancy remains unclear. Here, we quantify how ENSO persistently impedes mortality improvement, leading to considerable life expectancy and economic losses across high-income Pacific Rim countries. We estimate life expectancy losses of 0.5 years (monetary equivalent loss of $2.6 trillion) for the 1982–83 El Niño and 0.4 years ($4.7 trillion) for the 1997–98 event. Climate projections under moderate emission pathways suggest a cumulative decline of 2.8 years in life expectancy by 2100, amounting to $35 trillion losses, with most of the monetary burden falling on the middle-aged population. These findings reveal that intensifying ENSO variability poses an underrecognized and enduring threat to human health and socioeconomic stability, underscoring the urgent need for targeted adaptation strategies to safeguard population well-being.**

The El Niño–Southern Oscillation (ENSO) is Earth's most dominant year-to-year climate variation, integrating a wide range of Earth system processes[1,2]. ENSO involves fluctuations between unusually warm (El Niño) and cold (La Niña) sea surface temperatures in the central and eastern Pacific Ocean[1,3,4], triggering global weather extremes such as floods[5–7], heat extremes[8,9], and air pollution[10,11]. These weather extremes disrupt food security[12,13] and hinder economic growth[14,15]. ENSO has widespread, long-term impacts through its teleconnections, influencing multiple regions globally[16]. Many climate models predict that rising temperatures will intensify[17] and increase the frequency[18] of El Niño events, leading to severe socioeconomic consequences[19].

El Niño threatens human health, increasing mortality during event years[20–22]. It affects multiple health domains, including infectious and diarrheal diseases[23–26], cardiovascular and respiratory ailments[27,28], and healthcare system disruptions[26,29]. Vulnerable populations, such as children[12,30,31] and the elderly[32], face heightened risks, with El Niño events contributing to excess mortality. Emerging evidence suggests its health consequences extend beyond the event year, leading to long-term and compounding effects[33,34], although this has not been quantified. Most research focuses on past ENSO-related health outcomes or conceptual climate-health linkages, without rigorously quantifying their broader demographic and economic consequences. Here we bridge this gap by systematically quantifying ENSO-induced mortality and equivalent economic losses with a panel distributed lag regression framework.

We assess ENSO's impact on past and future mortality improvement across 10 Pacific Rim countries and regions (hereafter referred to as countries) with reliable mortality data from 1960 to 2022, calculating reductions in life expectancy and associated monetary loss. In this study, mortality improvement refers to the decline in mortality rates over time as public health improves, measured as the logarithmic year-over-year decline in age-specific mortality rates. ENSO intensity is captured using the E-index[35] (Methods), while country-level precipitation ($\tau^P$) and temperature ($\tau^T$) teleconnections quantify regional climate responses and are interacted with the E-index[14,15] (Methods) to isolate ENSO's influence. Focusing primarily on the five years following El Niño, we also analyze long-term impacts extending up to twenty years, including the effects of La Niña.

Finally, we integrate empirical estimates with climate model projections to assess the future life expectancy losses due to ENSO intensification in a warmer climate. By leveraging climate simulations under four emission scenarios, we analyze projected changes in ENSO and their potential impacts on life expectancy in the future (Methods).

## El Niño persistently deteriorates mortality improvement

El Niño events persistently slow the rate of mortality improvement (Fig. 1A). Mortality improvement is typically negative due to advancements in healthcare and living conditions[36]. A positive shift in mortality improvement suggests fewer lives are being saved compared to historical trends. Here, we demonstrate that ENSO disrupts mortality improvement, leading to increased mortality and reduced life expectancy. When ENSO intensity is zero, the mean mortality improvement is -2.1 percentage points (p.p.) (95% confidence interval [CI]: -2.3 to -1.9 p.p.), indicating a decline in all-age mortality in the Pacific Rim by 2.1 p.p. per year. However, five years after a 1-standard-deviation (s.d.) El Niño event, when the ENSO intensity was one, mortality improvement weakens to -0.6 p.p. (CI: -1.4 to 0.2 p.p.). This shift indicates a deterioration in human mortality outcomes, as more deaths are projected due to El Niño-related impacts. We found minimal evidence of endogeneity (Table S1) and identified three mediation pathways for both the immediate and cumulative horizon (Table S2), supporting a long-term causal link between ENSO and mortality improvement (Supplementary Materials).

The deterioration in mortality improvements remains robust across multiple checks, including alternative ENSO or teleconnection metrics, non–Pacific Rim samples, exclusion of post-COVID-19 years, removal of strongly teleconnected countries, and omission of economic controls (Figs. S1–3). The results also hold after accounting for intra-group correlation (Fig. S4) and heterogeneity across time, space, and demographics (Fig. S5). Leave-one-out resampling by year, age, or country confirms that no single group drives the results (Fig. S6). Non-linear distributed-lag models (Fig. S7) and phase-specific regressions (Fig. S8) further support robustness to non-linearity and asymmetry.

The impact of El Niño on mortality varies across age groups (Fig. 1B). The younger population (under 30) is the most affected, with a 1-s.d. El Niño event slowing mortality improvement by 3.0 p.p. (CI: 1.3 to 4.6) after five years. This heightened vulnerability likely reflects both greater environmental exposure and lower adaptive capacity. As a support to this interpretation, our causal-chain analysis (Table S2) shows that heat extremes, air pollution, and higher health expenditures significantly mediate El Niño's adverse effects on mortality improvement. These factors disproportionately affect younger individuals, who are more frequently engaged in outdoor labor and activities, increasing exposure to El Niño–driven stressors

such as heat extremes[37–39], and air pollution[10,11,40]. In addition, younger populations generally have fewer financial buffers and limited capacity to absorb El Niño–related increases in health expenditures, amplifying their long-term health risks. In comparison, the older population aged (60 and above) is the second most affected group (mean: 1.3 p.p., 95% CI: 0.8–1.8), consistent with reduced physiological resilience to environmental stressors. By contrast, those aged 30–59 years show the smallest but still measurable effect (mean: 0.3 p.p., 95% CI: –0.4–1.0), likely reflecting greater economic stability, healthcare access, and social support that buffer against climate-related health stresses.

Having established that El Niño persistently slows mortality improvement, a natural question arises: how long do these effects last? Our main analysis (Fig. 1) uses five lags to balance the long-term response to ENSO with statistical power, given the limited observational data. Models with additional lags reveal that El Niño effects can persist for 16 years or more, with a rebound around year 13 (Fig. S9). A second-order polynomial lag regression confirms that the baseline ENSO effect remains largely undiminished until around lag 13 before gradually weakening (Fig. S10). While longer-lag models improve data fit, they compromise model stability, suggesting that our five-lag specification provides a conservative estimate.

ENSO's impact on mortality likely varies by region and season. Examining seasonal teleconnections for each country shows that, although estimates generally overlap in their confidence intervals, winter and spring links are modestly stronger than summer, autumn, or the annual baseline (Fig. S2). To pinpoint timing, we focus on the contiguous U.S.—the most populous and data-rich country in our sample, with broad regional heterogeneity. Decomposing the results by state and month reveals a clear pattern: in northern states, where El Niño typically brings warmer, drier winters and springs, the cumulative impediment to mortality improvement concentrates in late summer to early winter; in southern states, where El Niño tends to be cooler, drier, the effect is concentrated in spring (Fig. S11).

## Life expectancy loss from historical El Niño's

The persistent effects of ENSO suggest that historical El Niño events have impacted life expectancy by slowing down mortality improvement. We examined the impact of the two largest El Niño events in the past 60 years—the 1982–83 (E-index=3.71) and 1997–98 (E=3.68) events–

–on life expectancy and calculated the equivalent monetary loss. The third largest event, in 2015–16 (E=2.71), is excluded from the main analyses as its five-year lag overlaps with the COVID-19 pandemic, but we report its impact in the Supplemental Materials (Fig. S12).

The effect on life expectancy is more complex than that on mortality improvement, as it also depends on a country's contemporary demographic profile (Methods). As El Niño events can trigger subsequent La Niña conditions[41], our analysis accounts for both the negative impacts of El Niño and the potential benefits of the following La Niña. Additionally, we employ a model that excludes the two major events, providing a better estimate of the effects of less extreme events (Fig. S1).

In the U.S., for example, the 1997–98 El Niño event caused a slowdown in mortality improvement, reducing life expectancy gains. Although this effect was partially offset by the consecutive La Niña events in 1999–2001, the 1997–98 El Niño still resulted in a loss of 0.44 years (CI: 0.10 to 0.78) (Fig. 2A) in life expectancy at birth. Without considering the consecutive La Niña events, the life expectancy at birth loss from the 1997–98 El Niño would have been 0.86 years (CI: 0.24 to 1.50) (Fig. 2A).

We estimated the population-weighted life expectancy at birth loss for the Pacific Rim countries from the 1982–83 and 1997–98 El Niño events to be 0.54 years (CI: 0.15 to 0.95) and 0.37 years (CI: 0.09 to 0.64), respectively (Fig. 2B). Despite being less intense, the 1982–83 event caused a larger loss than the 1997–98 event across countries (Fig. 2C). This discrepancy is due to the faster rate of mortality improvement during the 1982–83 period, making it more sensitive to proportional disruptions from the event.

## Valuing the economic cost of historical El Niño's

We estimated the monetary loss of the historical major El Niño events for each country using the value of statistical life approach (Methods).

Comparing the historical El Niño events reveals a pronounced escalation in the monetized impact of life expectancy loss over time. The aggregated life expectancy value losses for the 1982–83 and 1997–98 events are estimated at $2.6 trillion (95% CI: $0.8 to $4.4 trillion, 2020 dollars) and $4.7 trillion (95% CI: $1.3 to $8.0 trillion), respectively (Fig. 3B). Despite the 1982–83 event causing a larger decline in life expectancy across all countries in the sample (Fig. 2C), the 1997–

98 event resulted in substantially greater total losses in every country except Australia (Fig 3C). This discrepancy is attributed to a significant increase in value of statistical life (population-weighted from $2.0 million to $5.0 million, 2020 dollars), population growth, and a demographic shift toward middle-aged groups (Fig. 3A). For the same reason, the 2015–16 event produced the smallest loss in life expectancy among the three episodes (Fig. S12A), yet its aggregated economic loss is the largest (Fig. S12B), underscoring the growing economic weight of human life in an expanding and aging global population.

The monetary value of mortality losses peaks in midlife, driven by a combination of demographic and economic factors. First, the middle-aged cohort represents a larger share of the total population, amplifying aggregate losses. Second, life-expectancy reductions are proportionally greater for middle-aged adults than for older individuals, who already have limited remaining lifespans. Third, each midlife death carries greater welfare weight because it occurs during the prime working and earning years, when both individual productivity and household dependency are highest.

Two sources of uncertainty accompany the country-level valuations. First, statistical uncertainty in life-expectancy losses (Fig. 2C; regional CIs in Fig. 2B). Second, valuation uncertainty from country-specific value of statistical life (Methods). We report the country-specific economic cost valuation confidence range in Table S3. These disclosures make clear the limits of precision while supporting the robustness of the central conclusions.

**Projecting life expectancy and monetary loss from future ENSO intensification**

Building on historical analysis of ENSO's, we now examine its long-term impact on life expectancy in a warming climate and project future monetary loss. Using this empirical evidence, we now assess how future ENSO changes may amplify these losses under different climate and socioeconomic scenarios. We leverage global climate model simulations from the sixth phase of the Coupled Model Intercomparison Project (CMIP6) to analyze projected ENSO changes across four Shared Socioeconomic Pathways (SSPs), SSP1-2.6, SSP2-4.5, SSP3-7.0, and SSP5-8.5 (Methods).

CMIP6 projections show a 14–23% median increase in ENSO amplitude (Methods), with stronger El Niño events expected across all scenarios (Fig. 4C, D). The cumulative E-index for the

21st century is positive across all four SSP scenarios, with medians from 7.5 to 14.0 (Fig. 4C), and a median of 12.0 under SSP2-4.5, suggesting an overall intensification of ENSO variability. Alongside this El Niño dominance, the E-index time series shows substantial variability, reflecting ENSO's sensitivity to initial conditions[42] and its multidecadal variability[43]. Consequently, models and scenarios produce a wide range of E-index values, even with similar amplitude changes. For example, Fig. S13 illustrates that SSP2-4.5 simulations with comparable amplitude trends can exhibit different sequences of El Niño and La Niña events.

The total population of the countries in our sample is projected to increase by the end of the century under all SSPs, except for SSP3, suggesting a rise in overall population exposure (Fig. 4E). Additionally, the value of statistical life is projected to grow across all SSPs (Fig. 4G) due to projected monotonic growth in per capita gross domestic product (GDP) (Fig. 4F) (Methods). This trend suggests an increase in per capita exposure to mortality risk in the future. Based on these projections and empirical estimates, we quantify life expectancy losses with changes in ENSO. We calculated ENSO-related damages over 13 years, during which the damage accumulation is evident (Fig. S9, S16). This results in a conservative estimate of life expectancy impacts, which may vary across countries and age groups.

Climate projections of El Niño events under four SSPs result in substantial reductions in life expectancy and corresponding monetary losses throughout the 21st century (Fig. 4A, B). Under the average mortality improvement trend for each country and age group, and assuming a socioeconomic trajectory aligned with current greenhouse gas emission reduction pledges[44] (SSP2–4.5), the median cumulative life expectancy loss at birth from 2020 to 2099 is projected to be -2.8 years (Fig. 3A), with the 95% CI for SSP2–4.5 spanning -8.7 years to +0.4 years. Across all four scenarios, median losses range from -1.0 to -3.1 years. Additionally, the projected trajectory of life expectancy impact exhibits significant variation across individual simulations within each scenario (Fig. S14), reflecting the substantial variability in the E-index time series.

The monetary burden associated with life expectancy loss is substantial. Accounting for the future value of statistical life projections and applying a 3% discount rate[15], the median monetary loss equivalent to life expectancy reduction under SSP2–4.5 is estimated at $35 trillion. This amount represents approximately 1% of the total economic output of the countries covered over the 21st century, or nine times the U.S. national health expenditure in 2019 (the year before COVID-19). Across all four scenarios, median losses exceed $14 trillion. Alternative analytical

choices, including variations in income elasticity and different econometric approaches to value of statistical life estimation, do not alter the core finding of a substantial monetary burden associated with future life expectancy losses from ENSO (Fig. S15).

Although the projected median life expectancy loss for SSP3–7.0 is the greatest among all scenarios (Fig. 3A), the monetary burden associated with SSP3–7.0 remains lower than SSP2–4.5 and SSP5-8.5 (Fig. 3B). This discrepancy arises due to the lower projected population in SSP3–7.0, which reduces aggregate mortality-related economic losses. Additionally, the higher statistical value of life in SSP1–2.6 relative to SSP2–4.5 and SSP3–7.0 throughout the 21st century further influences the relative magnitude of the monetary burden across scenarios. For SSP5–8.5, however, both life expectancy loss and monetary burden show higher medians and greater variation compared to the other scenarios.

**Human cost of El Niño's and policy implications**

Our study demonstrates that El Niño persistently slows mortality improvement, resulting in substantial life expectancy losses and economic burdens, even across relatively wealthy countries. These mortality effects are most pronounced among younger populations (Fig. 1B), consistent with higher exposure to climate stressors and lower adaptive capacity[45], whereas the greatest economic burden falls on middle-aged individuals (Fig. 3B) because productivity losses are greatest[46], cohorts are larger, and remaining lifespans are shorter than for the young. Our findings imply that conventional mortality and economic forecasts may understate the true human cost of climate variability.

Placed within the broader ENSO–health literature, our findings complement event-window studies that emphasize short-term spikes during El Niño[20–22]. What we add is that these shocks propagate through multi-year lags, consistent with distributed-lag evidence of prolonged health effects from climate exposures[47–49]. This persistence shows that ENSO's health impacts accumulate over time, rather than being confined to immediate post-event years.

Policy implications follow directly. Because mitigation alone offers no clear near-term relief from ENSO-related mortality headwinds in the future climate (Fig. 4B), targeted adaptation is required. We suggest incorporating ENSO-sensitive indicators into public-health operations and labor protection, prioritizing regions and populations with high teleconnection exposure. Early-

warning[26], heat-health action plans, and climate-informed insurance design can reduce long-run losses and enhance resilience.

To balance interpretability with statistical power, we adopt a parsimonious lag specification and standard teleconnection measures. Sensitivity tests using alternative specifications (Figs. S1–S5) and generalized nonlinear distributed-lag frameworks (Figs. S7, S8) yield similar conclusions. Data gaps remain largest in lower-income settings where causal pathways may differ. Thus, we view our totals as conservative lower bounds. We call for the development of cause-specific, age-resolved, and intra-annual public health metrics, expended across income levels and regions, to support long-horizon attribution and better-targeted adaptation of ENSO-related public health challenges in a changing climate.

## Main References


1. McPhaden, M. J., Zebiak, S. E. & Glantz, M. H. ENSO as an integrating concept in earth science. *Science* **314**, 1740–1745 (2006).
2. Zebiak, S. E. *et al.* Investigating El Niño-Southern Oscillation and society relationships. *Wiley Interdiscip. Rev. Clim. Change* **6**, 17–34 (2015).
3. Philander, S., Pacanowski, R. & Yamagata, T. Unstable air-sea interactions in the tropics. *J. Atmos. Sci.* **41**, 604–613 (1984).
4. Wang, C. & Fiedler, P. C. ENSO variability and the eastern tropical Pacific: A review. *Prog. Oceanogr.* **69**, 239–266 (2006).
5. Ward, P., Kummu, M. & Lall, U. Flood frequencies and durations and their response to El Niño Southern Oscillation: Global analysis. *J. Hydrol.* **539**, 358–378 (2016).
6. Ward, P. J. *et al.* Strong influence of El Niño Southern Oscillation on flood risk around the world. *PNAS* **111**, 15659–15664 (2014).
7. Yang, Y. *et al.* Synchronization of global peak river discharge since the 1980s. *Nature Climate Change* 1–7 (2025).
8. Meehl, G. A., Tebaldi, C., Teng, H. & Peterson, T. C. Current and future US weather extremes and El Niño. *Geophys. Res. Lett.* **34**, L20704 (2007).
9. Gao, T., Luo, M., Lau, N.-C. & Chan, T. O. Spatially distinct effects of two El Niño types on summer heat extremes in China. *Geophys. Res. Lett.* **47**, e2020GL086982 (2020).
10. Jeong, J. I., Park, R. J. & Yeh, S.-W. Dissimilar effects of two El Niño types on PM2. 5 concentrations in East Asia. *Environmental Pollution* **242**, 1395–1403 (2018).
11. Marlier, M. E. *et al.* El Niño and health risks from landscape fire emissions in southeast Asia. *Nat. Clim. Chang.* **3**, 131–136 (2013).
12. Anttila-Hughes, J. K., Jina, A. S. & McCord, G. C. ENSO impacts child undernutrition in the global tropics. *Nat. Commun.* **12**, 5785 (2021).
13. Iizumi, T. *et al.* Impacts of El Niño Southern Oscillation on the global yields of major crops. *Nat. Commun.* **5**, 3712 (2014).
14. Callahan, C. W. & Mankin, J. S. Persistent effect of El Niño on global economic growth. *Science* **380**, 1064–1069 (2023).
15. Liu, Y., Cai, W., Lin, X., Li, Z. & Zhang, Y. Nonlinear El Niño impacts on the global economy under climate change. *Nat. Commun.* **14**, 5887 (2023).
16. Bjerknes, J. Atmospheric teleconnections from the equatorial Pacific. *Mon. Weather Rev.* **97**, 163–172 (1969).

17. Cai, W. *et al.* Increased variability of eastern Pacific El Niño under greenhouse warming. *Nature* **564**, 201–206 (2018).

18. Cai, W. *et al.* Increasing frequency of extreme El Niño events due to greenhouse warming. *Nat. Clim. Chang.* **4**, 111–116 (2014).

19. Cai, W. *et al.* Changing El Niño–Southern oscillation in a warming climate. *Nat. Rev. Earth Environ.* **2**, 628–644 (2021).

20. Kovats, R. S., Bouma, M. J., Hajat, S., Worrall, E. & Haines, A. El Niño and health. *Lancet* **362**, 1481–1489 (2003).

21. McGregor, G. R. & Ebi, K. El Niño Southern Oscillation (ENSO) and health: An overview for climate and health researchers. *Atmosphere* **9**, 282 (2018).

22. Anyamba, A. *et al.* Global disease outbreaks associated with the 2015–2016 El Niño event. *Sci. Rep.* **9**, 1930 (2019).

23. Stewart-Ibarra, A. M. & Lowe, R. Climate and non-climate drivers of dengue epidemics in southern coastal Ecuador. *Am. J. Trop. Med. Hyg.* **88**, 971 (2013).

24. Rosenberg, R. Vital signs: trends in reported vectorborne disease cases—United States and Territories, 2004–2016. *Morb. Mortal. Wkly. Rep.* **67**, 496–501 (2018).

25. Heaney, A. K., Shaman, J. & Alexander, K. A. El Niño-Southern oscillation and under-5 diarrhea in Botswana. *Nat. Commun.* **10**, 5798 (2019).

26. Ortiz-Prado, E. *et al.* El Niño-Southern Oscillation: a call to action for public health emergency preparedness and response. *Lancet Reg. Health-Am* **27**, 100601 (2023).

27. Tang, Q., Gong, K., Xiong, L., Dong, Y. & Xu, W. Can El niño–southern oscillation increase respiratory infectious diseases in China? An empirical study of 31 provinces. *Int. J. Environ. Res. Public Health* **19**, 2971 (2022).

28. Majeed, H., Moineddin, R. & Booth, G. L. Sea surface temperature variability and ischemic heart disease outcomes among older adults. *Sci. Rep.* **11**, 3402 (2021).

29. Aik, J. *et al.* Climate change and population health in Singapore: a systematic review. *Lancet Reg. Health-W. Pac.* **40**, 100947 (2023).

30. Aguilar, A. & Vicarelli, M. El Niño and children: Medium-term effects of early-life weather shocks on cognitive and health outcomes. *World Dev.* **150**, L20704 (2022).

31. Xu, H. *et al.* Maternal preconceptional and prenatal exposure to El Niño Southern Oscillation levels and child mortality: a multi-country study. *Nat. Commun.* **15**, 6034 (2024).

32. Xu, H. *et al.* Associations of climate variability driven by El Niño-southern oscillation with excess mortality and related medical costs in Chinese elderly. *Sci. Total Environ.* **851**, 158196 (2022).

33. Burton, C. *et al.* El Niño Driven Changes in Global Fire 2015/16. *Front. Earth Sci.* **8**, 199 (2020).

34. Chen, Y. *et al.* A pan-tropical cascade of fire driven by El Niño/Southern Oscillation. *Nat. Clim. Chang.* **7**, 906–911 (2017).

35. Takahashi, K., Montecinos, A., Goubanova, K. & Dewitte, B. ENSO regimes: Reinterpreting the canonical and Modoki El Niño. *Geophys. Res. Lett.* **38**, L10704 (2011).

36. Rischatsch, M., Pain, D., Ryan, D. & Chiu, Y. *Mortality Improvement: Understanding the Past and Framing the Future*. https://www.swissre.com/institute/research/sigma-research/sigma-2018-06.html (2018).

37. Ebi, K. L. *et al.* Hot weather and heat extremes: health risks. *Lancet* **398**, 698–708 (2021).

38. Mora, C. *et al.* Global risk of deadly heat. *Nature climate change* **7**, 501–506 (2017).

39. Vicedo-Cabrera, A. M. *et al.* The burden of heat-related mortality attributable to recent human-induced climate change. *Nature climate change* **11**, 492–500 (2021).

40. Chang, L., Xu, J., Tie, X. & Wu, J. Impact of the 2015 El Niño event on winter air quality in China. *Sci. Rep.* **6**, 34275 (2016).

41. Cai, W. *et al.* Increased frequency of extreme La Niña events under greenhouse warming. *Nat. Clim. Chang.* **5**, 132–137 (2015).

42. Cai, W. *et al.* Butterfly effect and a self-modulating El Niño response to global warming. *Nature* **585**, 68–73 (2020).

43. Callahan, C. W. *et al.* Robust decrease in El Niño/Southern Oscillation amplitude under long-term warming. *Nat. Clim. Chang.* **11**, 752–757 (2021).

44. Meinshausen, M. *et al.* Realization of Paris Agreement pledges may limit warming just below 2°C. *Nature* **604**, 304–309 (2022).

45. Health, Wellbeing and the Changing Structure of Communities. in *Climate Change 2022 – Impacts, Adaptation and Vulnerability: Working Group II Contribution to the Sixth Assessment Report of the Intergovernmental Panel on Climate Change* (ed. Intergovernmental Panel on Climate Change (IPCC)) 1041–1170 (Cambridge University Press, Cambridge, 2023). doi:10.1017/9781009325844.009.

46. Burke, M., Hsiang, S. M. & Miguel, E. Global non-linear effect of temperature on economic production. *Nature* **527**, 235–239 (2015).

47. Armstrong, B. *et al.* Longer-Term Impact of High and Low Temperature on Mortality: An International Study to Clarify Length of Mortality Displacement. *Environmental Health Perspectives* vol. 125 (2017).

48. Gasparrini, A. *et al.* Mortality risk attributable to high and low ambient temperature: a multicountry observational study. *Lancet* vol. 386 369–375 (2015).

49. Young, R. & Hsiang, S. Mortality caused by tropical cyclones in the United States. *Nature* **635**, 121–128 (2024).

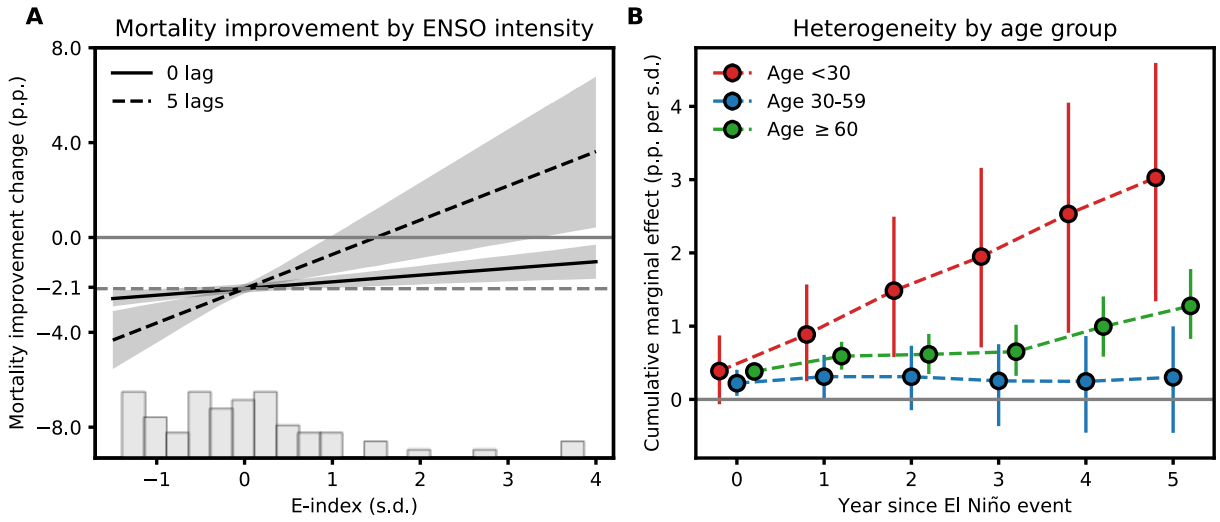



**Fig. 1. ENSO's lag effect on mortality improvement.**

(**A**) Mortality changes by varying ENSO intensities in the year of the event (zero lag, solid line) and the fifth year after the event (5 lags, dashed line). The black lines represent the mean, while the shaded areas indicate the 95% confidence intervals from bootstrap resampling (Methods). The positive shift in mortality indicates a deterioration in human mortality improvement, as more people are projected to die because of El Niño-related impacts. When ENSO intensity is zero, the mean mortality change is -2.1%, as Pacific Rim countries, on average, experienced mortality improvement over the research period. The lower histogram shows the density of the E-index in the sample. (**B**) Cumulative effects of a 1-s.d. El Niño event over time, beginning with the year of the event (year 0) and accumulating to the fifth year after the event (year 5). The population is segmented into three age categories. Dots show averages, and bars show 95% CIs. p.p., percentage points; s.d., standard deviation.

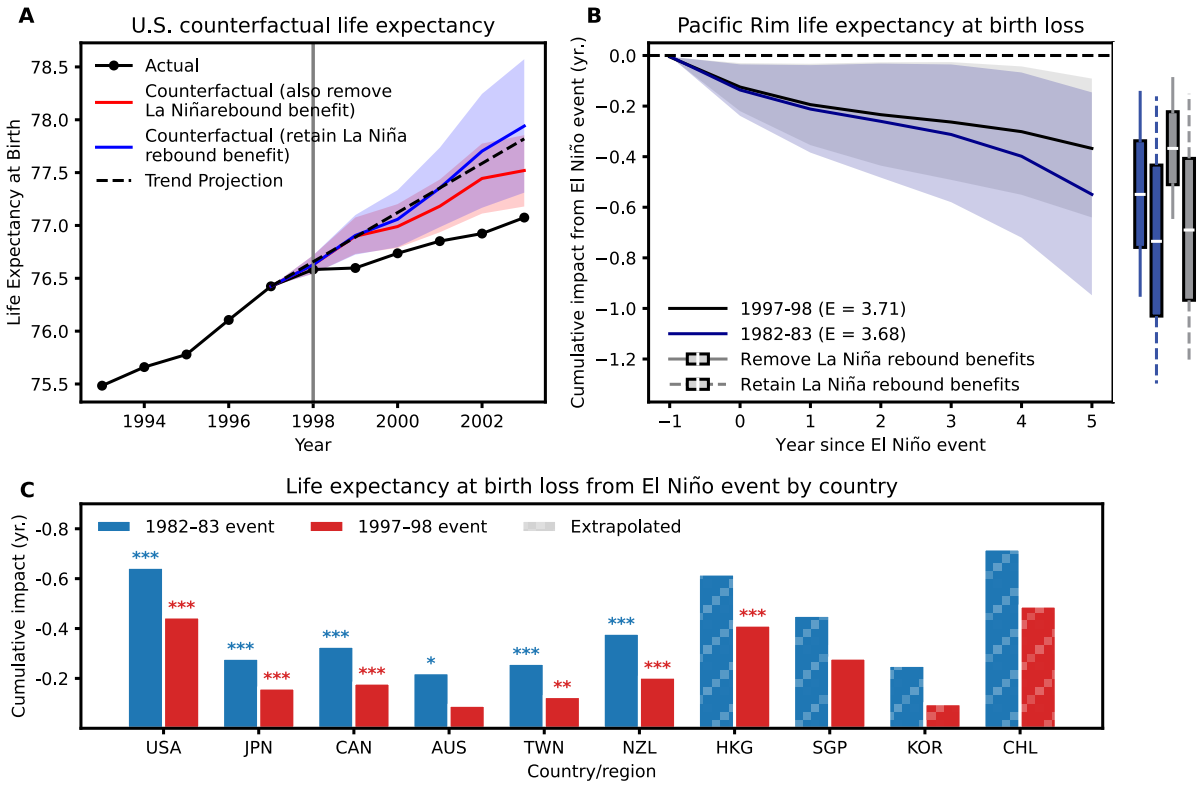



**Fig. 2. Persistence of El Niño effects on life expectancy.**

(**A**) Counterfactual life expectancy at birth in the U.S. around the 1997–98 El Niño event. The actual life expectancy (black) is compared to two counterfactuals: one removes both the El Niño effect and the post-event La Niña rebound benefit (red), and one removes only the El Niño effect while retaining the post-event La Niña rebound benefit (blue). Shaded areas show 95% CIs. Dashed line represents projected life expectancy assuming pre-El Niño trends continued. (**B**) Cumulative Pacific Rim life expectancy changes for the 1982–83 (blue) and 1997–98 (black) El Niño events. Central line shows the mean, and shading shows the 95% CIs. December-January-February E-index for the corresponding years is reported in the legend. Boxplots compare the two counterfactual definitions: remove El Niño and La Niña rebound benefit (solid); remove El Niño, retain La Niña rebound benefit (dashed). (**C**) Country- / region-level five-year cumulative loss in life expectancy at birth for the 1982–83 (blue) and 1997–98 (gray) events. Hatched bars denote estimates that rely on extrapolated mortality data for that country. Asterisks mark statistical significance (*** $p < 0.01$, ** $p < 0.05$, * $p < 0.10$). Statistical significance is not reported for extrapolated estimates. Bars extend upward in a negative direction to indicate larger losses.

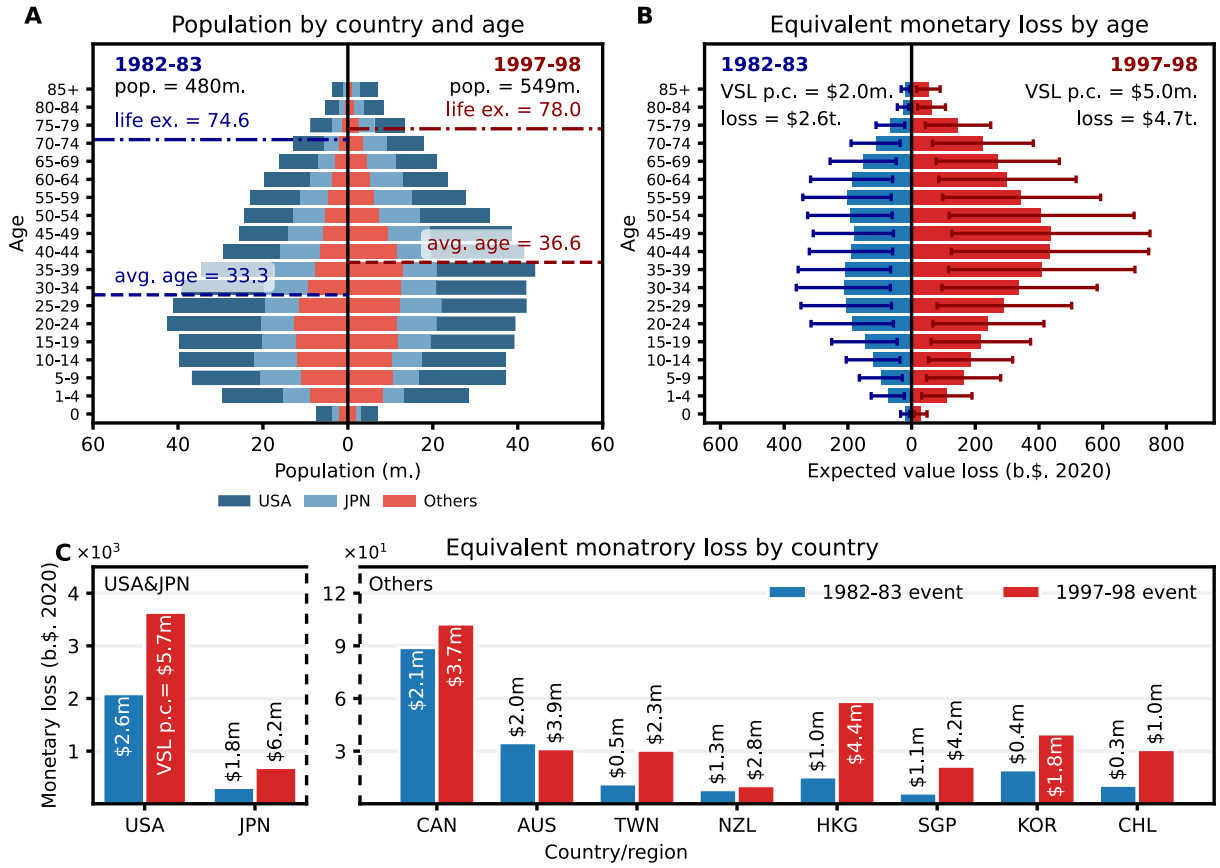



**Fig. 3. Economic cost of El Niño induced life expectancy losses.**

(**A**) Population by country/region and age in 1983 (left of the vertical axis) and 1998 (right). Colors group the population into USA, Japan, and Others. Horizontal dashed lines mark average age and life expectancy; in-panel labels report totals. (**B**) Age-specific expected monetary loss (billions, 2020 USD) from each event, shown as mirrored bars with 95% confidence intervals. The 1982–83 event is in blue and 1997–98 in gray; in-panel labels report event-year value of statistical life per capita (VSL p.c.) and total loss. (**C**) Country-/region-level VSL loss (billions, 2020 USD). Left: USA & Japan (note the $\times 10^3$ scale). Right: other locations ($\times 10^1$ scale). Bars compare the losses of each country (billion USD) for 1982–83 (blue) and 1997–98 (gray) events; numeric labels inside bars indicate the event-year VSL p.c. (million USD).

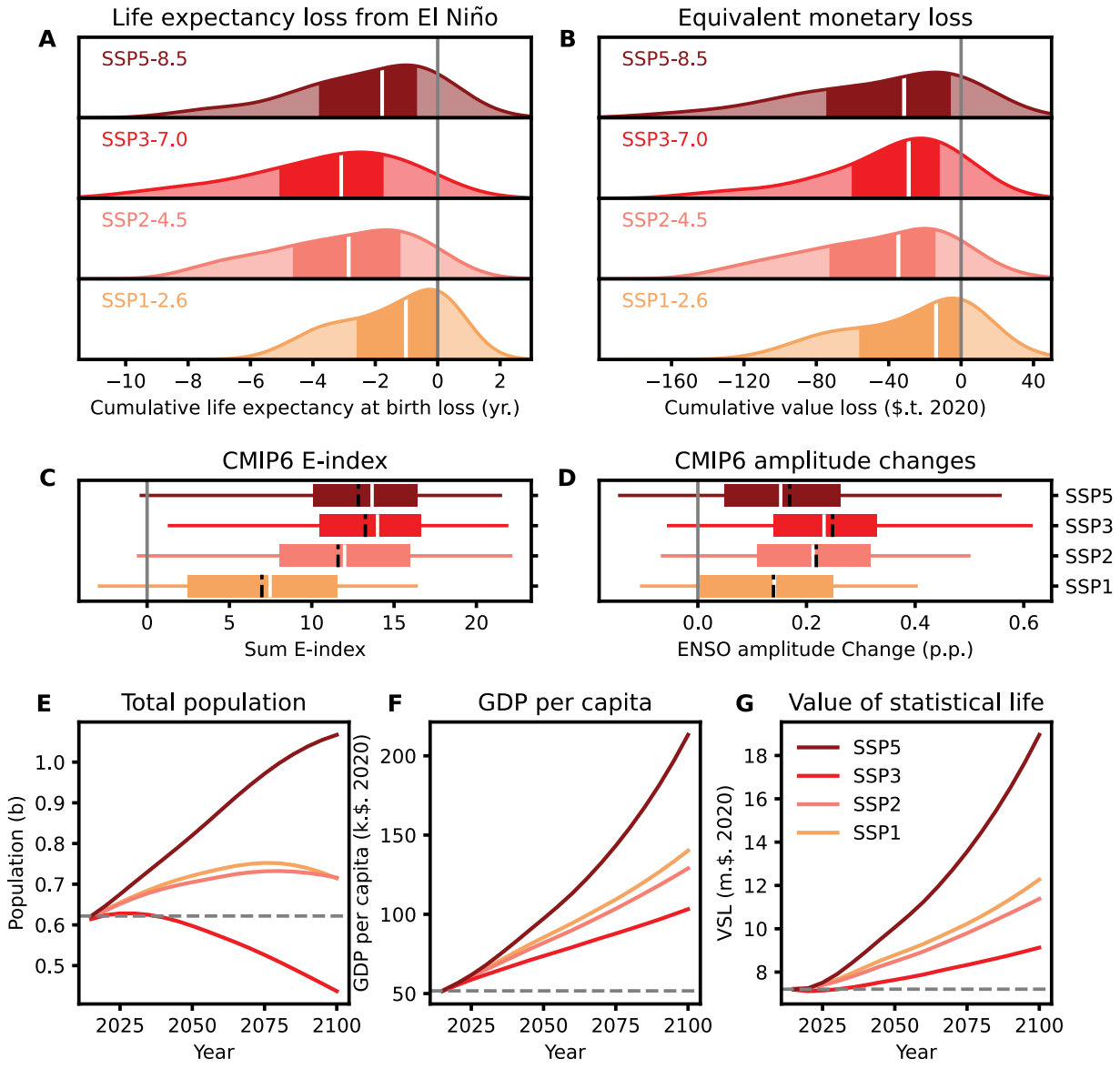



**Fig. 4. Projected life expectancy loss and equivalent economic loss from ENSO.**

(**A**) Probability distribution of the projected life expectancy loss in 2099, accumulated from ENSO impacts over the period 2020–2099. The data is derived from an ensemble of 200 CMIP6 simulations from four SSPs. In each panel, the darker area represents the interquartile range (first to third quartile), and the white line denotes the median value of the distribution. (**B**) Cumulative equivalent monetary loss from 2020 to 2099, represented using the same format as (**A**). Change in ENSO amplitude between 1940–2015 and 2020–2099 (**C**) and sum of E-index of 2020–2099 (**D**) for an ensemble of 200 CMIP6 simulations from four SSPs. Box indicates the interquartile range, and whisker indicates the range between the 5th and 95th percentile. Also shown is the multi-model ensemble median (solid white) and mean (dashed black) for each scenario. (**E**–**G**) Projections of total population, per capita gross domestic product (GDP; measured in purchasing power parity), and population-weighted value of statistical life (VSL) from 2015 to 2099. The grey dashed lines represent the corresponding baseline VSL value in 2015.

# Methods

## Mortality data

We use nationally representative total-population mortality data for Pacific Rim countries and regions: Australia, Canada, Chile, Japan, New Zealand, the Republic of Korea, Taiwan, the U.S., Singapore, and Hong Kong SAR. Mortality data for Singapore are obtained from the Singapore Department of Statistics[50], while data for the other countries comes from the Human Mortality Database (HMD)[51,52]. For the United States, we additionally use state-level data from the U.S. Human Mortality Database (USHMD)[53] , which follows the same structure and quality standards as HMD. This dataset provides coherent regional coverage and consistent definitions across countries. All mortality tables use 5×1 (age × year) intervals with annual mortality rate for age 0, 1–4, and subsequent five-year age groups from 5–9 up to 105-109, with an open-ended 110+ group (90+ for Singapore).

## Economic data

As El Niño creates significant macroeconomic disruptions[14,46,54], we utilized a wide range of country-level economic and health spending data from the Organisation for Economic Co-operation and Development (OECD)[55] and the International Monetary Fund (IMF)[56] to rule out the effect of economic slowdowns on human mortality disruptions[57].

We acquire health spending data as a percentage of Gross Domestic Product (GDP) from the OECD. Macroeconomic data at the country-year level, including GDP, GDP per capita, inflation rate (average consumer price index), and unemployment rate, are sourced from the IMF, while interest rate data is obtained from the OECD. Additionally, we obtain microeconomic data, such as the Business Confidence Index and the Consumer Confidence Index, from the OECD.

To support a sub-national analysis, we obtain state-level economic data for the U.S., including personal income per capita and the unemployment rate, from the Federal Reserve Economic Data[58].

## Historical meteorological data

We acquire monthly land temperature data from the Berkeley Earth dataset[59], sea surface temperature (SST) data from the Hadley Centre Sea Ice and Sea Surface Temperature dataset (HadISST)[60], and precipitation data from the Global Precipitation Climatology Center (GPCC)[61].

The Berkeley Earth and GPCC datasets are processed and aggregated into a structured format at the country level. HadISST dataset is at a 1º×1º latitude-longitude grid resolution.

**Shared socioeconomic pathways data**

Climate model data is derived from the sixth phase of the Climate Model Intercomparison Project (CMIP6)[62]. We utilize historical and projected monthly SST (variable label "tos"), monthly surface air temperature ("tas"), and monthly precipitation ("pr") data spanning from 1850 to 2099, combining historical simulations with projections under the Scenario Model Intercomparison Project (SSPs; SSP1-2.6, SSP2-4.5, SSP3-7.0, and SSP5-8.5). These scenarios cover a broad spectrum of potential future policies, from significant mitigation efforts (SSP1-2.6) to scenarios of continued high emissions (SSP5-8.5). The projected increase in global mean temperatures by 2081-2100, relative to 1995-2014, is approximately 1.2ºC for SSP1-2.6, 2.1ºC for SSP2-4.5, 3.2ºC for SSP3-7.0, and 4ºC for SSP5-8.5[62,63].

**Contextual benchmarks**

We use two authoritative sources for context only (not for model estimation). First, global disaster losses are taken from the WMO Atlas of Mortality and Economic Losses from Weather, Climate and Water Extremes (1970–2019)[64]. Second, U.S. health-care expenditure series are taken from the CDC/NCHS Health Care Expenditures data page[65].

**ENSO intensity measure**

To quantify ENSO's effects, we use two commonly employed indices: the E-index and the C-index. The E-index represents the variability of SST anomalies in the eastern Pacific, associated with the canonical ENSO pattern where warming occurs primarily in the eastern equatorial Pacific[35,66]. The C-index, a companion to the E-index, represents central Pacific ENSO events, with La Niña trends typically being stronger. Positive E-index values indicate an eastern Pacific El Niño event, while negative C-index values indicate a central Pacific La Niña event. We focus on E-index and C-index as primary indicators of ENSO variability because they are widely established in the literature for distinguishing eastern Pacific and central Pacific ENSO events, respectively. Their complementary coverage allows us to capture spatial heterogeneity in SST anomalies and the differential climate impacts across the Pacific Ocean Basin[14,35,42,66–68].

The E-index and C-index are derived from the first two principal components (PCs) of an empirical orthogonal function (EOF) analysis applied to Pacific SSTs[14,35] over the region 20ºS to 20ºN and 140ºE to 80ºW for the period 1960–2022. When applied to SST data, EOF analysis identifies dominant spatial patterns and their associated time series. The leading EOFs capture the primary modes of variability, helping to distinguish between different climate phenomena such as El Niño. After performing EOF analysis on SST anomalies, the first two principal components (PC1 and PC2) are obtained, representing the time evolution of the leading EOFs.

$$E = \frac{PC1 - PC2}{\sqrt{2}}, \text{ and } C = \frac{PC1 + PC2}{\sqrt{2}} \quad \text{(S1)}$$

For a given year, we average the E-index over the winter months (December to February (of next year), DJF) to focus on the season in which ENSO peaks[68]. The results are shown in Fig. S16. To assess the robustness of our results to alternative ENSO indices, we also calculated the Niño 3 and Niño 3.4 indices. The Niño 3 region (5°N–5°S, 150°W–90°W) and the Niño 3.4 region (5°N–5°S, 170°W–120°W) are both widely used for monitoring ENSO activity.

For climate projections, we calculate the December-January-February (DJF) E and C-indices similarly in the CMIP6 models, using quadratically detrended SST anomalies referenced to monthly means from 1850–2014.

We find that the C-index and its teleconnections play a less significant role in human mortality improvement inferences relative to the E-index (Fig. S3). This finding is consistent with recent literature on the enduring effects of El Niño on economic growth[14,66]. Therefore, we excluded the C-index and its teleconnections from our model to save some degrees of freedom, focusing instead on the impact of eastern Pacific El Niño events (measured by the E-index) on human mortality improvement in this study.

**ENSO teleconnections**

Our analysis of El Niño's impact on human mortality improvement uses a country-specific teleconnection metric to quantify the heterogeneity in a country's geophysical connection to ENSO. We standardize the country-level mean surface temperature and precipitation by subtracting the long-term (1960–2022) monthly mean and dividing by the long-term monthly standard deviation. We then linearly detrend these standardized anomalies to remove the effects of warming and low-frequency climate variability.

The country-level teleconnections are then calculated by correlating the standardized temperature and precipitation time series with the DJF E-index separately for each month and each country[14,15]. El Niño events begin and grow in year *t*-1, peak in the winter, and then decay and disappear in the spring and summer of year *t*[69]. Therefore, we allow the DJF E-index to affect both the preceding (from June of year *t*-1) and the following years (to August of year *t*). The DJF period is widely recognized as the peak season for ENSO events, when both SST anomalies atmospheric teleconnections reach their maximum intensity. Accordingly, averaging ENSO indices over DJF is a standard approach in climate research[70]. This calculation yields a distribution of 15 correlation coefficients (one per month from June of year *t*-1 through August of year *t*) for each country, for both temperature and precipitation (see Fig. S22). We then compute the maximum absolute value of the 3-month rolling correlation to capture the period of strongest teleconnection response. These values are then used to represent each country's E-index temperature and precipitation teleconnections, denoted as $\tau^T$ and $\tau^P$, respectively.

**Mortality improvement**

For age interval *x* and year *t*, let the observed mortality rate be $m_{xt}$. Mortality improvement is the logarithmic difference between the current and previous mortality rate:

$$a_{xt} = \log\left[m_{xt}\right] - \log\left[m_{x(t-1)}\right]. \tag{S2}$$

Form the econometric methods discussed later, we estimate the ENSO-attributed effect $\Delta_{xt}$ and remove it to obtain the counterfactual improvement $\hat{a}_{xt}$:

$$\hat{a}_{xt} = a_{xt} - \Delta_{xt}. \tag{S3}$$

Counterfactual mortality rates are then reconstructed recursively:

$$\hat{m}_{xt} = \begin{cases} \hat{m}_{x(t-1)} \cdot \exp\left[\hat{a}_{xt}\right] & \text{for } t > t_0, \\ m_{xt} & \text{for } t = t_0. \end{cases} \tag{S4}$$

Observed and counterfactual schedules are converted to life expectancy using standard life-table methods (Supplementary Materials).

Here, $t_0$ denotes the starting year where the impact of extreme ENSO events on mortality is removed. We set $t_0$ to the year before the event in the single-event analysis (Figs. 2, S12) and to 2015 for CMIP6 projections (Fig. 4).

## Econometric model

We estimate the enduring effect of ENSO on mortality improvement using a panel distributed-lag model with country–age fixed effects:

$$a_{ixt} = \sum_{l=0}^{L} \left( \beta_{0l} + \beta_{1l} \cdot \tau_i^P + \beta_{2l} \cdot \tau_i^T \right) E_{t-l} + Controls_{it} + u_{ix} + \varepsilon_{ixt} . \quad \text{(S5)}$$

Here, we index the mortality improvement for country $i$, age group $x$, and year $t$ as $a_{ixt}$, adding a country index $i$ compared Eq (S2). $E_t$ represents the E-index in year $t$. The interaction of $E_t$ with $\tau_i^T$ and $\tau_i^P$ allows the effect of ENSO to vary between countries based on the extent to which each country's temperature and precipitation are coupled with ENSO. We use control variables to isolate the influence of ENSO from other time-varying factors affecting mortality improvement. To account for baseline differences between country-age groups, we include a country-age fixed effect denoted as $u_{ix}$, ensuring our results are identified using within-country-age variation in mortality improvement. We do not include a year-fixed effect in our baseline model, as the E-index is a cross-sectional constant within each year. Instead, we include a pandemic dummy to account for the impact of COVID–19 from 2020 to 2022. However, other time-varying factors may still be correlated with ENSO and influence the results. As an additional robustness check, we group years into 5-year intervals, include these groups as time-fixed effects, and find that the core results remain robust (Fig. S5).

The distributed lag regression model enables us to distinguish whether El Niño's impact on mortality improvement is short-term or enduring. If El Niño only causes a temporary disruption in human mortality through channels such as increased incidence rates, a shock in year $t$ would be followed by a recovery in year $t$+1, with mortality improvement rates rebounding to their original trajectory. This would result in a significant increase in mortality improvement in year $t$+1. Conversely, if El Niño affects the long-term capacity for mortality improvement, the years following an event should show either persistent declines in growth or no change.

Therefore, our analysis focuses on cumulative coefficients $\Theta_{iL}$ , which represent the accumulated effect of ENSO in the years following a shock:

$$\Theta_{iL} = \sum_{l=0}^{L} \left( \beta_{0l} + \beta_{1l} \cdot \tau_i^P + \beta_{2l} \cdot \tau_i^T \right) . \quad \text{(S6)}$$

If $\Theta_{iL}$ is significantly different from zero, we can reject the hypothesis that El Niño has only a short-term effect. Conversely, enduring effects are identified if $\Theta_{iL}$ is significantly different from zero. The interaction of $E_t$ with $\Theta_{iL}$ allows us to calculate the cumulative effect for each country $i$ over lag length $L$. Multicollinearity tests show that including multiple E-index lags do not damage the regression (Table S4).

To mitigate the influence of occasional outliers, we employed bootstrap resampling to assess the statistical significance of the ENSO impact. Specifically, we performed 1,000 resampling iterations from a uniform distribution with replacement. Additionally, we conducted resampling by grouping the data at different levels, including country, year, age, and country-age in 5-year intervals. The results remain robust across these resampling settings (Fig. S4).

**Climate model selection**

Many climate models struggle to realistically represent the physical processes driving ENSO[71,72]. To address this, previous studies have proposed a method to filter the physically realistic models by calculating the quadratic coefficient ($\alpha$ parameter) in the relationship between PC1 and PC2 from the EOF analysis used to calculate the E and C-indices[42,66]. The observed $\alpha$ parameter is -0.34, indicating a strong nonlinearity in the principal component space and a clear distinction between eastern Pacific and central Pacific El Niño[14]. Following Cai et al.[66], we adopted the selection criteria $\alpha$ <-0.17 to identify climate simulations with realistic ENSO representations. Using this approach, we selected 267 simulation ensembles from MIROC6[73], MIROC-ES2L[74], MPI-ESM1-2-LR[75], and EC-Earth3[76] across four SSPs (61 for SSP1-2.6, 82 for SSP2-4.5, 62 for SSP3-7.0 and 62 for SSP5-8.5), offering robustness for our study.

**Life expectancy loss from historical extreme El Niño events**

The regression coefficients $\beta_{il}$ ($i$ = 0, …, 2, $l$ = 0, …, $L$) derived from the Equation (S5) can be interpreted as the impact on human mortality improvement for a one standard deviation change in the E-index. We apply these coefficients to the actual and historical E-index values to calculate the life expectancy loss from specific historical El Niño events.

We develop a "counterfactual" E-index time series, wherein these events did not occur by setting the corresponding E-index values (1983, 1998, 2016) to zero.[14] Using the regression coefficients, we calculate the impact on mortality improvement by comparing the actual and

counterfactual time series. Formally, if $E_t$ represents the observed E-index in the event year $t$, and $\hat{E}_t$ represents the counterfactual E-index in that year, we calculate the change in mortality improvement for country $i$ and age group $x$ in year $t+l$ as:

$$\Delta_{ix(t+l)} = \left(\beta_{ol} + \beta_{1l} \cdot \tau_i^P + \beta_{2l} \cdot \tau_i^T\right) \cdot \left(E_t - \hat{E}_t\right). \quad \text{(S7)}$$

We then calculate the counterfactual mortality improvement $\hat{a}_{ix(t+l)}$ for year $t+l$ following Equation (S2). The actual and counterfactual life expectancy from the event year to five years after the event can then be determined using the methods described in the life expectancy section of this supplementary material.

The above analysis considers only the impact of El Niño events. However, El Niño events can dynamically trigger La Niña events, which have beneficial effects. To fully account for the effects of El Niño, it is necessary to include these offsetting beneficial events. For instance, the 1982–83 El Niño may have triggered the major La Niña of 1984–85 (with E-index values of -0.5 in 1984 and -1.1 in 1985), and the 1997–98 El Niño may have triggered the major La Niña of 1999–2000 (with E-index values of -0.6 in 1999 and -1.4 in 2000) (Fig. S16). We incorporate these beneficial effects for both El Niño events by setting the E-index to zero for the five-year window and calculating the disruption in mortality improvement and the loss in life expectancy. As a result, the life expectancy loss is further reduced by accounting for the benefits of La Niña.

**Projected life expectancy loss from future ENSO intensification**

To represent a climate scenario without increased ENSO intensity, following Callahan and Mankin[14], we calculate a counterfactual E-index by adjusting each simulation's projection time series to match its historical period amplitude. For instance, if a model projects a 20% increase in the E-index amplitude, we adjust its future time series by reducing it by 20%, preserving the sequence of ENSO events but removing the intensity increase. We then estimate mortality improvements by comparing each year's future and counterfactual E-index for each realization between 2020 and 2099. We calculate the cumulative impact as the difference between the future and counterfactual E-index, as described in Eq. (S7).

**Monetary value of historical life expectancy loss**

We estimate the monetary burden of life expectancy loss from historical El Niño events using a willingness-to-pay approach, specifically the value of statistical life (VSL) method. VSL is a widely used concept in health economics and policy for quantifying the trade-off between income and the risk of death[77–80].

We adopt the U.S. Department of Health and Human Services (HHS) 2020 VSL estimate of $11.4 million (2020 dollars) as the baseline. HHS VSL is derived from the Census of Fatal Occupational Injuries (CFOI) data and adjusted for known biases[77]. Country and year specific VSLs are obtained with scaling by income[77–82].

$$VSL_{it} = VSL_{USA,2020} \cdot \left( \frac{GNIPC_{it}}{GNIPC_{USA,2020}} \right)^{\xi}, \tag{S8}$$

where $i$ and $t$ index country and year, respectively. The parameter $\xi$ represents the income elasticity, which measures the percentage change in VSL associated with a 1% change in real income. Consistent with literature common practice[77,83,84] and the recommendation of HHS[81], we choose $\xi = 1$, and report sensitives for $\xi = 0.5$, 1.5 (historical events: Table S1; future SSPs: Fig. S15).

Following previous research on the valuation of changes in life expectancy[77,85], we covert VSL to the value of a statistical life year (VSLY) to estimate the economic value of life years lost due to El Niño. The VSLY is derived by distributing the VSL over the remaining life expectancy at the average age ($e_{i\bar{x}t}$) without discounting[77,85]:

$$VSLY_{it} = VSL_{it} / e_{i\bar{x}t}. \tag{S9}$$

The country-age-year monetary loss is then:

$$Loss_{ixt} = VSLY_{it} \cdot \left( \hat{e}_{ixt} - e_{ixt} \right) \cdot \exp\left( -re_{ixt} \right), \tag{S10}$$

Using the realized life expectancy ($e_{ixt}$) and counterfactual life expectancy ($\hat{e}_{ixt}$) derived from corresponding mortality rates (Supplemental Materials).

**Project monetary value of future life expectancy loss**

The key component in projecting the future monetary burden of life expectancy loss from El Niño, as estimated from climate simulations, is the projection of future incomes under different socioeconomic scenarios (Equations (S8)).

We estimate GNI for each scenario using GDP (PPP) projections. The validity of this approach is supported by historical data, where intra-country GDP-to-GNI ratios remain generally stable over time (Fig. S17). This method has been applied in previous works[77]. However, in some countries, the GDP-to-GNI ratio exhibits an upward trend (Fig. S18). We identify these trends as statistically significant for Australia, Chile, Japan, the Republic of Korea, New Zealand, Singapore, and the United States (Table S5). To account for these variations, we allow the GDP-to-GNI ratio to vary dynamically over time based on the observed trends. This enables us to estimate future GNI trajectories under different climate scenarios. By incorporating projected population changes across scenarios, we further derive GNIPC estimates for each country and year under the respective socioeconomic pathways. Given the projected GNIPC for each country and year, we derive future VSL estimates and the corresponding monetary burden using Equations (S8) , (S9), and (S10).

**Methods References**


50. Singapore Department of Statistics. Death and Life Expectancy Publications and Methodology. (2024).

51. Human Mortality Database. Max Planck Institute for Demographic Research, University of California, Berkeley, and French Institute for Demographic Studies (2024).

52. Barbieri, M. *et al.* Data Resource Profile: The Human Mortality Database (HMD). *Int. J. Epidemiol.* **44**, 1549–1556 (2015).

53. United States Mortality DataBase. University of California, Berkeley (USA) (2024).

54. Hsiang, S. M. & Meng, K. C. Tropical economics. *Am. Econ. Rev.* **105**, 257–261 (2015).

55. OECD Data. Organisation for Economic Co-operation and Development (2024).

56. IMF Data. International Monetary Fund (2024).

57. Cutler, D. M., Huang, W. & Lleras-Muney, A. *Economic Conditions and Mortality: Evidence from 200 Years of Data*. https://www.nber.org/papers/w22690 (2016).

58. FRED Economic Data. Federal Reserve Economic (2024).

59. Rohde, R. A. & Hausfather, Z. The Berkeley Earth land/ocean temperature record. *Earth Syst. Sci. Data* **12**, 3469–3479 (2020).

60. Rayner, N. *et al.* Global analyses of sea surface temperature, sea ice, and night marine air temperature since the late nineteenth century. *J. Geophys. Res.-Atmos.* **108**, ACL (2003).

61. Schneider, U. *et al.* GPCC full data reanalysis version 7.0: Monthly land-surface precipitation from rain gauges built on GTS based and historic data. UCAR/NCAR-Research Data Archive (2016).

62. O'Neill, B. C. *et al.* The Scenario Model Intercomparison Project (ScenarioMIP) for CMIP6. *Geosci. Model Dev.* **9**, 3461–3482 (2016).

63. Tebaldi, C. *et al.* Climate model projections from the scenario model intercomparison project (ScenarioMIP) of CMIP6. *Earth Syst. Dynam.* **12**, 253–293 (2021).

64. Douris, J. & Kim, G. *WMO Atlas of Mortality and Economic Losses from Weather, Climate and Water Extremes (1970–2019)*. https://wmo.int/publication-series/wmo-atlas-of-mortality-and-economic-losses-from-weather-climate-and-water-extremes-1970-2019 (2021).

65. Centers for Disease Control and Prevention. *Health Care Expenditures*. https://www.cdc.gov/nchs/hus/topics/health-care-expenditures.htm (2023).

66. Cai, W. *et al.* Increased ENSO sea surface temperature variability under four IPCC emission scenarios. *Nat. Clim. Chang.* **12**, 228–231 (2022).

67. Jia, F., Cai, W., Gan, B., Wu, L. & Di Lorenzo, E. Enhanced North pacific impact on El Niño/southern oscillation under greenhouse warming. *Nat. Clim. Chang.* **11**, 840–847 (2021).

68. Ng, B., Cai, W., Cowan, T. & Bi, D. Impacts of Low-Frequency Internal Climate Variability and Greenhouse Warming on El Niño–Southern Oscillation. *J. Clim.* **34**, 2205–2218 (2021).

69. Larkin, N. K. & Harrison, D. E. On the definition of El Niño and associated seasonal average US weather anomalies. *Geophysical Research Letters* **32**, (2005).

70. Yeh, S.-W., Wang, G., Cai, W. & Park, R. J. Diversity of ENSO-Related Surface Temperature Response in Future Projection in CMIP6 Climate Models: Climate Change Scenario Versus ENSO Intensity. *Geophysical Research Letters* **49**, e2021GL096135 (2022).

71. Karamperidou, C., Jin, F.-F. & Conroy, J. L. The importance of ENSO nonlinearities in tropical pacific response to external forcing. *Clim. Dyn.* **49**, 2695–2704 (2017).

72. Seager, R. *et al.* Strengthening tropical Pacific zonal sea surface temperature gradient consistent with rising greenhouse gases. *Nat. Clim. Chang.* **9**, 517–522 (2019).

73. Tatebe, H. *et al.* Description and basic evaluation of simulated mean state, internal variability, and climate sensitivity in MIROC6. *Geosci. Model Dev.* **12**, 2727–2765 (2019).

74. Hajima, T. *et al.* Development of the MIROC-ES2L Earth system model and the evaluation of biogeochemical processes and feedbacks. *Geoscientific Model Development* **13**, 2197–2244 (2020).

75. Mauritsen, T. *et al.* Developments in the MPI-M Earth System Model version 1.2 (MPI-ESM1. 2) and its response to increasing CO2. *Journal of Advances in Modeling Earth Systems* **11**, 998–1038 (2019).

76. Döscher, R. *et al.* The EC-earth3 Earth system model for the climate model intercomparison project 6. *Geoscientific Model Development Discussions* **2021**, 1–90 (2021).

77. Nandi, A. *et al.* Global and regional projections of the economic burden of Alzheimer's disease and related dementias from 2019 to 2050: A value of statistical life approach. *EClinicalMedicine* **51**, 101580 (2022).

78. Viscusi, W. K. & Masterman, C. J. Income elasticities and global values of a statistical life. *J. Benefit-Cost Anal.* **8**, 226–250 (2017).

79. Aldy, J. E. & Viscusi, W. K. Adjusting the value of a statistical life for age and cohort effects. *Rev. Econ. Stat.* **90**, 573–581 (2008).

80. Scott, A. J., Ellison, M. & Sinclair, D. A. The economic value of targeting aging. *Nat. Aging* **1**, 616–623 (2021).

81. *Appendix D: Updating Value per Statistical Life (VSL) Estimates for Inflation and Changes in Real Income*. https://aspe.hhs.gov/reports/updating-vsl-estimates (2021).

82. Viscusi, W. K. & Aldy, J. E. The value of a statistical life: a critical review of market estimates throughout the world. *J. Risk Uncertain.* **27**, 5–76 (2003).

83. Carlson, C. J. *et al.* Health losses attributed to anthropogenic climate change. *Nature Climate Change* 1–4 (2025).

84. Sun, Y. *et al.* Global supply chains amplify economic costs of future extreme heat risk. *Nature* **627**, 797–804 (2024).

85. Robinson, L. A., Hammitt, J. K. & O'Keeffe, L. Valuing mortality risk reductions in global benefit-cost analysis. *J. Benefit-Cost Anal.* **10**, 15–50 (2019).

## Supplementary Materials

Supplementary Text

Figs. S1 to S23

Tables S1 to S10

# Supplementary Materials for

## Enduring impacts of El Niño on life expectancy in past and future climates

**Authors:** Yanbin Xu[1]*, Wenjun Zhu[1], Dhrubajyoti Samanta[2], Benjamin P. Horton[3]*

**Affiliations:**

[1]Department of Banking and Finance, Nanyang Business School, Nanyang Technological University; Singapore.

[2]Earth Observatory of Singapore, Nanyang Technological University; Singapore.

[3]School of Energy and Environment, City University of Hong Kong; Hong Kong SAR

*Corresponding author. Email: yanbin.xu@ntu.edu.sg, bphorton@cityu.edu.hk

### Life expectancy

To derive the life expectancy from mortality, we utilize a life table method. The procedure is the same for observed and counterfactual life expectancy; thus, we use the observed life expectancy (denoted as $e_{xt}$) to illustrate. Our analysis of columns of life tables follows the actuarial convention. See Table S6 for an illustration of the typical structure of a life table.

The probability of death $q_{xt}$ represents the death probability within the age interval $x$ to $x$+1. From the $m_{xt}$, we obtain $q_{xt}$ as below, assuming a uniform distribution of death over the age interval:

$$q_{xt} = \frac{n_x m_{xt}}{1 + \frac{n_x}{2} m_{xt}}, \quad \text{(S11)}$$

where $n_x$ represents the length of the age interval of $x$ (e.g., for age group 10-14, $n_x$ = 5).

Human mortality rates exhibit a distinctive pattern across different age intervals. Using US mortality data as an example (Fig. S19). Initially, mortality rates are high during infancy (under 1

year) due to congenital conditions, infections, and complications during childbirth. Following this period, the mortality rate drops significantly and remains low throughout childhood (1 to 14 years), a time characterized by high levels of health and survival. During adolescence and young adulthood (15 to 35 years), mortality rates continue to be low but will exhibit a mortality hump due to external causes such as accidents, drug overdose, and risky behaviors. In middle age (35 to 64 years), mortality rates gradually increase as individuals begin to experience the effects of aging, including chronic diseases like heart disease and cancer. The most significant rise in mortality rates occurs in old age (above 65 years), driven by a higher prevalence of chronic illnesses and decreased physiological resilience[86].

However, a phenomenon known as the "mortality plateau" is observed, where beyond a certain age, the probability of dying in a given year stabilizes rather than continuing to increase exponentially[87]. This phenomenon, likely driven by data limitations, remains a subject of scientific debate and research. To mitigate the potential noise caused by the mortality plateau in our results, we focus on mortality improvement samples up to the 80- to 84-year-old age interval. For ages 85–89 and above, we do not make a counterfactual adjustment for the mortality rates but directly use the observed $m_x$ to calculate $q_x$ and derive life expectancy. This makes the life expectancy loss estimation more country-specific and captures potential late-age variations associated with ENSO that were not considered in the previous counterfactual mortality reconstruction.

We denote the number of survivors of age $x$ at the beginning of year $t$ as $l_{xt}$. The number of deaths in year $t$ between the age interval $x$ and $x+1$ is denoted as $d_{xt}$. The calculations for $l_{xt}$ and $d_{xt}$ are as follows:

$$l_{xt} = \begin{cases} l_{(x-1)t} - d_{(x-1)t} & \text{for } x > x_0, \\ 100,000 & \text{for } x = x_0; \end{cases} \tag{S12}$$

$$d_{xt} = q_{xt} \cdot l_{xt}. \tag{S13}$$

In Equation (S12), $x_0$ denotes the age interval under 1 year old, as we set $l_{xt}$ for the first age interval (under one year old) at 100,000. For the other age intervals, $l_{xt}$ is calculated as the number of survivors minus the number of deaths in the previous age interval. Meanwhile, $d_{xt}$ is calculated as the expected number of individuals that will die in the current age interval.

The total number of person-years lived within the age interval $x$ for year $t$ is denoted as $L_{xt}$, and it is approximated as follows:

$$L_{xt} = \left[ l_{xt} - \frac{d_{xt}}{2} \right] \cdot n_x \tag{S14}$$

Here, $l_{xt}$ is reduced by half of $d_{xt}$ before being weighted by the number of years within the current age interval, $n_x$, to linearly approximate the number of deaths occurring within the interval, which is an approach that is widely accepted in the actuarial science discipline[88].

We denote $T_{xt}$ as the expected total number of person-years that the cohort lives from age $x$ onwards:

$$T_{xt} = \sum_{x' \geq x} L_{x't} \,. \tag{S15}$$

Finally, the life expectancy at age $x$ in year $t$, denoted as $e_{xt}$ , is calculated as the expected total number of person-years that the cohort lives from age $x$ onwards, divided by the number of survivors at age $x$ in year $t$:

$$e_{xt} = \frac{T_{xt}}{l_{xt}} \,. \tag{S16}$$

Table S6 provides a stylized representation of the life table method used to calculate life expectancy from the mortality rate. Using this method, we calculate the observed life expectancy $e_{xt}$ and the counterfactual life expectancy $\hat{e}_{xt}$ from $m_{xt}$ and $\hat{m}_{xt}$ , respectively. The life expectancy loss is then determined as the difference between $\hat{e}_{xt}$ and $e_{xt}$ .

**Addressing ENSO endogeneity**

ENSO's impact on mortality improvement raises endogeneity concerns, as it functions as a macroeconomic factor[89], while economic growth and individual income are also linked to mortality rates[90,91].

To address endogeneity concerns, we applied a threefold causal identification analysis. First, we comprehensively include lagged macro- and microeconomic variables (see Method) and employ country-age level fixed effects to account for country-specific trends in our main model. This comprehensive approach to economic controls limits the chance of omitted variable bias. Additionally, using lagged economic variables, rather than contemporaneous ones, helps avoid forward-looking bias in the analysis.

Second, we test the correlation between ENSO's impact on economic growth and its impact on mortality improvement, finding an insignificant correlation. Specifically, we observe a correlation of -0.19 ($p$-value = 0.61) between ENSO's country-specific effects on mortality improvement and its impact on economic growth (Fig. S20). Given the possibility that this insignificant correlation may be due to limited observations at the country level, we extended the analysis to the state level in the continental U.S., estimating ENSO's impact on both income growth and mortality improvement. At the state level, the correlation between the impact on income growth and mortality improvement is -0.04 ($p$-value = 0.80). While this does not fully rule out potential endogeneity concerns, the insignificant correlation suggests that economic growth and income growth are unlikely to be omitted variables causing endogeneity in the relationship between ENSO and mortality improvement.

Third, to further address the possibility of omitted variables that are correlated with ENSO and affect human mortality improvement, we employ a Two-Stage Least Squares regression approach using lagged monthly sea-level pressure as an instrumental variable. The results indicate that endogeneity concerns between ENSO and mortality improvement are limited. As shown in Table S1, in the first stage, the SP-index is statistically significant at the 0.01 level, and the Cragg-Donald Wald F-statistic is high ($p$-value < 0.01), confirming that the instrument is valid and strong. In the second stage, the estimated coefficients retain the same sign and magnitude as in the main results, with statistical significance maintained across lags 0 to 5. Additionally, the overidentification test ($p$-value = 1.00) suggests that there are no overidentification issues.

The analyses suggest that endogeneity concerns are minimal and further support the causal interpretation of ENSO's effects on mortality improvement.

**Singapore special adjustment**

The Singapore mortality data from the Department of Statistics, covering 1990–2022, follow the same age and time interval definitions as the Human Mortality Database (HMD) Specifically, $m_x$ for age 0, age group 1–4, and subsequent five-year age groups from 5–9 up to 80–84. The dataset also includes mortality rates for age 85–89 (from year 2000 onward) and a single grouped rate for ages 90 and above. In contrast, HMD reports five-year age groups up to 105–109 and aggregates only the 110+ group.

As our analysis of El Niño's enduring effects on mortality improvement (Fig. 1 and its robustness tests) focuses on age groups up to 80–84 (to avoid the noise associated with mortality plateaus at very old ages), no adjustments were required for the Singapore mortality data itself.

When calculating life expectancy (Fig. 2) for Singapore, we extended the life table to age 110+ by setting $q_x = 1$ at age 110 (assuming all remaining individuals die by that age) and linearly extrapolated $q_x$ for age groups 85–89, 90–94, 95–99, 100–104, and 105–109 between the observed $q_x$ for 80–84 and the assumed terminal value at 110+. Although this introduces a minor assumption for the oldest ages, the effect is minimal because individuals aged 85+ account for only about 0.7% of Singapore's population, and Singapore itself represents an annual average of 0.8% of the total population in our analysis sample.

**Life expectancy loss and monetary equivalent loss of 2015-16 El Niño**

As the 2015–16 El Niño event temporally overlapped with the COVID-19 pandemic, we did not include its life expectancy and economic impacts in the main manuscript but evaluated them as a robustness check. Although the initial exclusion was motivated by this overlap, we acknowledge that the episode provides a useful point of comparison. Specifically, we estimated the change in life expectancy and the corresponding economic loss for the Pacific Rim region over the five-year window following the 2015–16 event under two scenarios: (1) an observed case and (2) a case that excludes the COVID-19 effect.

The first scenario, which compares the observed trajectory with a counterfactual removing both the El Niño effect and the subsequent La Niña rebound benefit, follows the same methodology used to generate Fig. 3. In the second scenario, we first excluded the country- and age-specific COVID-19 effects before removing the El Niño signal. To construct the COVID-19–excluded baseline, we calculated the age-specific average mortality improvement over 2010–2019 for each country and extrapolated the expected mortality rates for 2020 and 2021. The El Niño counterfactual against this baseline further removed the El Niño effect and its post-event La Niña rebound benefit.

The resulting life-expectancy losses were 0.33 years in the observed case and 0.31 years when excluding the COVID-19 effect (Fig. S12A), with corresponding economic losses of USD 10.7 trillion and USD 10.1 trillion (2020 values) (Fig. S12B), respectively. The age-specific loss patterns remain consistent with those reported for the 1982–83 and 1997–98 events (Fig. 3), with middle-aged populations bearing the largest impacts.

## Causal chain through health stressors

We examine the causal chain linking ENSO to mortality improvement through three plausible health-stress mechanisms identified in the literature: two physical stressors (air pollution and heat extremes) and one socioeconomic stressor (health expenditure).

The two physical stressors are (1) air pollution, measured by surface-level PM2.5 concentrations, and (2) heat extremes, measured by the annual maximum daily temperature (TXx). The PM2.5 data was obtained from World Health Organization Air quality database 2022 (V5), while the TXx data was obtained from the Berkly Earth dataset. Previous studies have shown that El Niño events can elevate PM2.5 concentrations through intensified biomass burning[11] and altered atmospheric circulation patterns,[10,40] thereby increasing respiratory[92] and cardiovascular[93] mortality risk that lasts in long-term. Similarly, extreme heat has been associated with excess mortality[38,94] and El Niño.[8,9] Although long-term mortality effects of extreme heat have not been firmly established, we included this variable as a key ENSO-sensitive stressor given its relevance to ongoing climate change.

The socioeconomic stressor is national health expenditure growth, which reflects both adaptive capacity and economic response. Unlike physical stressors, this variable may exhibit two-way causality—higher mortality risks can lead to increased contemporaneous health spending for the same year. To mitigate this potential endogeneity, we tested the effect of ENSO on health expenditure in the current year and its influence on mortality improvement in the following year, thereby reducing forward-looking bias.

To evaluate these mechanisms, we employed a structural equation modeling framework[95,96], testing the indirect (mediated), direct, and total effects of ENSO on mortality improvement via the three stress pathways. The results are presented in Table S1, and distinct mediation patterns are shown:

- Health expenditure: ENSO significantly increases short-term health spending (Panel A, col. 1), which offsets approximately –11.6% [95% CI: –32.6% to –3.1%] of the mortality-impairing effect, likely reflecting households' adaptive spending responses. However, cumulatively, ENSO reduces health expenditure over five years (Panel A, col. 2), explaining 10.4% [95% CI: 2.4% to 29.2%] of the long-term slowdown in mortality improvement, consistent with its potential macroeconomic consequences.

- Air pollution (PM2.5): The short-term mediation effect is not statistically significant, but cumulatively it explains 6.1% [90% CI: 0.2% to 17.7%] of the observed ENSO-related slowdown in mortality improvement.
- Heat extremes (TXx): The immediate-year mediation effect accounts for 14.6% [90% CI: 4.2% to 62.2%] of the ENSO impact, whereas the five-year cumulative effect is not significant, consistent with prior findings that heat risk itself is primarily immediate.[38]

As a robustness check, we also repeated the analysis using rural PM2.5 and Tx5d[97] (temperature of the hottest 5-day heat wave in each year) as alternative metrics for air pollution and heat extremes, respectively. The results were qualitatively consistent with those in Table S1. Overall, our findings suggest that ENSO generally slows down human mortality improvement through its effects on environmental and socioeconomic health stressors. These results highlight the need for future research on region-specific and cause-specific pathways linking ENSO to long-term health outcomes.

**Enduring effect of La Niña**

Our baseline specification assumes a linear, symmetric relationship between the E-index and mortality improvement—implicitly treating La Niña (negative E-index) as generally beneficial to health. To test whether La Niña effects are underrepresented, we allow nonlinearity and asymmetry by separating El Niño and La Niña signals in Equation (S5) and comparing three alternative specifications:

- Two-mode (asymmetric) model. Decompose the E-index as $EN_{t-l}$ = max ($E_{t-l}$, 0), and a $LN_{t-l}$ = min ($E_{t-l}$, 0), and estimate separate coefficients for $EN_{t-l}$ and $LN_{t-l}$ (and their interactions), allowing distinct El Niño vs. La Niña responses.
- One-mode models. Estimate two regressions that include only $EN_{t-l}$ or only $LN_{t-l}$, respectively, to isolate each side's effect without the other in the equation.
- Quadratic model. Augment the baseline with a quadratic term in E-index (and quadratic terms for the teleconnection interactions) to capture curvature in the exposure–response function.

This framework tests both directional asymmetry and nonlinear curvature in the ENSO–mortality relationship.

Across all three, El Niño events were found to gradually impede mortality improvement, while La Niña events tended to enhance it from lag 0 to 5 (Fig. S7A, B). The marginal-effect plots (Fig. S7C–H) further show that the two phases generally exert opposing effects at most lags, with some concurrent impediment observed at years 3 and 5.

In addition, in Supplemental Material Section "Robustness test with distributed lag non-linear model", we tested nine specifications of non-linear exposure–response and lag-response pairs and found that the five-year cumulative effects are reversed between El Niño (positive E-index) and La Niña (negative E-index) phases, with some specifications reporting non-significant La Niña impacts and others showing modest benefits (Fig. S8).

Taken together, these analyses do not rule out La Niña–related impediments. Instead, they suggest that, in aggregate, cumulatively, El Niño exerts a predominantly negative influence on mortality improvement, whereas La Niña is, on average, associated with favorable outcomes.

**Robustness test with distributed lag non-linear models**

We relax the linearity assumption on the lag structure by reassessing the ENSO-mortality improvement relation under a distributed lag non-linear model (DLNM) framework[98,99]. The DLNM approach flexibly captures non-linear exposure–response and lag–response relationships while preserving the temporal coherence of cumulative effects.

We evaluated all nine combinations of lag and exposure bases:

- Lag bases: (1) natural cubic spline [represented as: NS (df = 3)], (2) quadratic polynomial [Poly (df = 2)], and (3) linear [Linear].
- Exposure bases: (1) natural cubic spline with knots at the 50th and 90th percentiles [NS knots P50/P90], natural cubic spline (df = 3) [NS (df = 3)], and quadratic polynomial [Poly (df = 2)].

The best-fitting specification, based on the lowest AIC, applies a second-order polynomial exposure term with a linear lag term (Fig. S8G). This model predicts slightly larger El Niño impediments and stronger La Niña benefits relative to the baseline distributed lag model, but the estimates mostly remain within overlapping confidence bounds.

**Sensitivity to additional lags**

To assess how long El Niño can impede improvements in human mortality, we extended the lag structure of our baseline distributed lag regression model. The results indicate that the adverse effects can persist for up to 16 years, with a rebound beginning around year 13 (Fig. S9). Including additional lags improves model fit up to roughly 20 lags, beyond which the limited sample length begins to reduce statistical power.

When splitting the population into cohorts born before or after the El Niño event, we observe distinct temporal patterns in the cumulative mortality response (Fig. S9F). The pre-event cohort shows a more persistent deterioration in mortality improvement that lasts for up to 16 years after the event, whereas the post-event cohort exhibits a relatively stronger but statistically insignificant and short-lived effect. Although we cannot definitively determine whether ENSO's impact on mortality deterioration is permanent due to limited observational data, the findings for the pre-event cohort indicate long-term effects that persist for at least 16 years.

We further employed a second-order polynomial distributed lag model—the best-performing specification in our tests under the DLNM framework. This model offers a good statistical performance and clear interpretability, as it captures the overall shape of the lag response while substantially reducing the number of estimated parameters and preserving statistical power.

In this framework, the lag response coefficients of the baseline econometric model (Eq. S5) are constrained by a quadratic polynomial,

$$\begin{cases} \beta_{0\ell} = \theta_{00} + \theta_{01}\ell + \theta_{02}\ell^2 \\ \beta_{1\ell} = \theta_{10} + \theta_{11}\ell + \theta_{12}\ell^2 \\ \beta_{2\ell} = \theta_{20} + \theta_{21}\ell + \theta_{22}\ell^2 \end{cases}, \qquad l = 0,...,L\,.$$

Define the polynomial-weighted sums of the E-index:

$$Z_{0t} = \sum_{l=0}^{L} E_{t-l}\,,\; Z_{1t} = \sum_{l=0}^{L} E_{t-l}\cdot l\,,\; Z_{2t} = \sum_{l=0}^{L} E_{t-l}\cdot l^2\,.$$

The collapsed regression of Equation (S5) is then

$$a_{ixt} = \sum_{k=0}^{2} (\theta_{k0} + \theta_{k1}\cdot \tau_i^{\mathrm{P}} + \theta_{k2}\cdot \tau_i^{\mathrm{T}}) Z_{kt} + Controls_{it} + u_{ix} + \varepsilon_{ixt}\,. \tag{S17}$$

Rather than estimating the individual lag coefficients $\{(\beta_{0l}, \beta_{1l}, \beta_{2l})\}_{l=0}^{L}$ directly, the second order polynomial lag regression model estimates the shape parameters $\{(\theta_{0k}, \theta_{1k}, \theta_{2k})\}_{k=0}^{2}$ and recovers the implied lag response. This preserves degrees of freedom when $L$ is large, at a cost in flexibility.

Interpretation follows from the shape parameters: The intercept term ($\theta_0 = \theta_{00} + \theta_{10} \cdot \tau^T + \theta_{20} \cdot \tau^P$) represents the average baseline effect of ENSO across lags, the slope term ($\theta_1 = \theta_{01} + \theta_{11} \cdot \tau^T + \theta_{21} \cdot \tau^P$) captures the direction and persistence of the lagged response over time, and the curvature term ($\theta_2 = \theta_{02} + \theta_{12} \cdot \tau^T + \theta_{22} \cdot \tau^P$) reflects the acceleration or deceleration of this effect—indicating whether ENSO's influence intensifies or weakens at longer horizons. Using this specification, we extended the lag horizon to 40 years (about two-thirds of our sample period), with results shown in Fig. S10.

As shown in Fig. S10, the estimated coefficients remain broadly stable across extended lags. The average baseline effect ($\theta_0$) persists until approximately lag 29 (Fig. S10A). The slope term ($\theta_1$) remains insignificant until lag 13, then turns negatively significant, indicating that El Niño persistently impedes mortality improvement until lag 13 before a gradual rebound (Fig. S10B). The curvature term ($\theta_2$) becomes positively significant around lag 18, indicating the rebound effect gradually flattens thereafter (Fig. S10C). These results are generally consistent with the additional lag checks with the baseline model (Fig. S9).

Overall, these results reinforce the robustness of our findings and indicate that including up to 16 lags provides a reasonable and conservative representation of the cumulative ENSO impact on mortality improvement, consistent with the observed persistence of El Niño's effects for more than 16 years.

**Sensitivity to early year under-registration**

Our sample spans 1960–2022, during which part of the sea surface temperature data prior to 1981 were based on station observations rather than satellite retrievals[100]. To assess potential under-registration or data-quality issues in the earlier period, we repeated our baseline analysis after excluding the first one-third of the sample and compared the results with the full-sample estimates. As shown in Fig. S1D, the estimated ENSO impacts on mortality improvement are slightly reduced but remain qualitatively consistent and within the confidence interval of the full-sample results. This suggests that potential early-period data limitations do not materially affect our main findings.

**Sensitivity to teleconnection**

To assess the sensitivity of our baseline results to the teleconnection metric, we replicated the analysis using two alternatives:

(1) Mean correlation (Mean Corr.): the average of the 15 monthly correlations between the DJF E-index and each country's monthly temperature or precipitation anomaly; and

(2) Regression-based (Reg.): the coefficient from regressing monthly anomalies on the E-index.

Model fits for all three definitions are compared in Table S7. The baseline (extreme 3-month rolling correlation) provides the best fit, as indicated by the lowest AICc, suggesting a more realistic representation of ENSO–mortality linkages. Separately for temperature and precipitation, the baseline metric is positively and approximately linearly associated with both alternatives (Fig. S2A, B). As shown in Fig. S2C, estimates across metrics differ slightly but remain within one another's 95% CIs, confirming consistency.

We also evaluated seasonal teleconnections by averaging monthly correlations within winter, spring, summer, and autumn (with hemisphere adjustments for Australia and New Zealand). Results are broadly similar across seasons, with slightly stronger responses in winter and spring; all estimates fall within confidence ranges (Fig. S2D).

**Multicollinearity test**

Using lags in regression might lead to potentially multicollinearity results due to the autocorrelation of the lags. To address this concern, we conducted three checks to assess this issue.

First, we examined the autocorrelation among E-index lags, reported in Table S4 (columns 1–5). The highest absolute correlation was observed between $E_{t-4}$ and $E_{t-5}$ (–0.372), which is well below commonly accepted thresholds. Following standard econometric references[101,102], correlations below 0.8 are generally considered safe, and those below 0.5 are regarded as highly acceptable. Thus, this correlation test preliminarily suggests that multicollinearity among lag terms is minimal.

Second, to further verify this, we computed the Variance Inflation Factors (VIFs) for all lagged E-index variables (Table S4, column 7). The two highest VIFs were 1.70 ($E_{t-2}$) and 1.65 ($E_{t-3}$), far below the conservative threshold of 10 commonly cited in[101] and Kennedy[102]. Since the minimum possible VIF is 1 (indicating no collinearity), these values confirm that multicollinearity does not materially affect our model. Unlike pairwise correlations, the VIF test captures joint linear dependencies across all lag terms, providing a more comprehensive diagnostic.

Third, our results with the DLNM framework use significantly fewer coefficients to estimate the lag effect. These results (Fig. S8) further support the robustness of our findings to potential multicollinearity concerns.

Together, these tests indicate that the inclusion of multiple E-index lags does not introduce harmful multicollinearity, ensuring stable and interpretable coefficient estimates in our distributed-lag specifications.

**Regional and monthly breakdown in the continental U.S.**

ENSO likely influences human mortality through heterogeneous regional and seasonal pathways. While our robustness test on seasonal teleconnection reported in "Sensitivity to teleconnection" addresses seasonal sensitivity, we further examined the localized and time-specific nature of ENSO's effects using state-month–level mortality data for the continental U.S.

We focused on the U.S. because monthly mortality data at subnational levels are largely unavailable for other countries. The U.S., however, provides a suitable test case due to its large population size, diverse climatic regions, and reliable vital statistics. The sample period spans 2000–2019, chosen to avoid potential coding inconsistencies from the ICD-9 to ICD-10 transition in 1999 and to exclude COVID-19 disruptions after 2020. To construct monthly, age-specific state mortality estimates at the state level, we combine CDC death records, which provide monthly counts of death by age and state, and USHMD data, which contains annual mortality rates. For each state-year, we calculated the monthly proportion of deaths by each age group using CDC data and then allocated the USHMD annual mortality rate accordingly to derive monthly, age-specific mortality rates. To minimize volatility from small counts, we excluded state-age groups with fewer than 1,000 annual deaths in low-population states—though our results remain robust when retaining younger groups for large states.

We began by visualizing state-level seasonal ENSO teleconnections (Fig. S21). The results reveal clear north–south contrasts in temperature and precipitation anomalies during El Niño events, approximately divided by 40°N. Northern states tend to be warmer and drier in winter and spring, whereas southern states are generally cooler and wetter. During summer and autumn, temperature anomalies weaken, and most states show neutral precipitation responses. Based on this observed climatological divide, we grouped states into northern (>40°N) and southern (<40°N) categories to evaluate seasonal heterogeneity in ENSO's mortality effects.

Both regions experience reduced mortality risk during El Niño winters in the immediate year (Fig. S11A), though this short-term benefit largely dissipates within five years (Fig. S11B). In the southern states, El Niño more strongly impedes mortality improvement, particularly during spring and summer, whereas in the northern states, most of the cumulative effects occur in spring and remain weaker in magnitude. Overall, while immediate effects are not statistically different between regions, the southern states exhibit stronger cumulative impacts, with mean and median effects still within the confidence bounds of the national sample.

These findings demonstrate that ENSO's influence on mortality improvement varies across both time of year and region. In the U.S. context, warmer and drier northern states during El Niño winters show smaller cumulative mortality impediments, whereas cooler and wetter southern states experience more substantial and persistent impacts extending into summer and autumn. Future research using similar subnational datasets in other regions could further unravel the location- and season-specific mechanisms through which ENSO influences human mortality.

**Two-stage Least Square**

The rationale for using sea-level pressure (SLP) as an instrumental variable lies in its role as an exogenous determinant of El Niño events. SLP drives atmospheric conditions that influence the development and intensity of El Niño but is not directly affected by economic conditions or mortality outcomes. By using SLP as an instrumental variable, we isolate the variation in El Niño that is independent of potential confounding economic and mortality factors. This isolation allows for a more accurate estimation of El Niño's causal impact on human mortality improvement. The two-stage least squares approach further strengthens our methodology by addressing omitted variable bias, ensuring that the observed relationship between El Niño and mortality outcomes is not spuriously influenced by unobserved economic variables.

Specifically, we apply Principal Component Analysis to the matrix of SLP, where the rows represent time steps, and the columns represent each 1º×1º grid over the region from 20ºS to 20ºN and 140ºE to 80ºW. We extract the first principal component, which serves as a time-series representation of SLP at a monthly frequency. For each year $t$, we use the average SLP from March to May (MAM) of the year $t-1$ as the independent variable in the first-stage OLS model, with the E-index as the dependent variable. The first-stage OLS model predicts the E-index using the independent variable, and this predicted E-index is then substituted for the observed E-index in the econometric model to refit Equation (S5).

## Central Pacific ENSO

Our empirical model uses the E-index as the ENSO intensity measure, reflecting the eastern Pacific ENSO[35] (Methods). We also tested the C-index, which measures the central Pacific ENSO, alongside the E-index. Using the C-index alone (Fig. S3A) shows a short-term mortality impact lasting two years, likely due to the high correlation between the E- and C-indices (0.74, Table S4), followed by a rebound after the third year. In the dual-index model (Fig. S3B), the central Pacific La Niña shows a slight reduction in mortality after five years, but this effect is not statistically significant. The inclusion of the C-index increases the regression coefficients for the E-index, suggesting that our main analysis provides more conservative estimates.

## Generalization of the results

Despite the consistent deterioration in mortality across countries (Fig. S20) and model specifications (Fig. S1), we acknowledge that our sample may may be subject to some bias. Most countries covered by the HMD are relatively high-income, with comprehensive population and mortality data, while lower-income countries are underrepresented due to limited data availability. As such, our estimates may represent a conservative lower bound for the total global impact of ENSO on mortality.

The nature and mechanisms of mortality impacts may also differ across income contexts. In high-income countries, heat stress and air quality degradation are likely the dominant pathways, whereas in lower-income countries, waterborne diseases, food insecurity, and vector-borne illnesses may play a greater role[103]. These distinct pathways imply that while the magnitude of losses may be amplified in lower-income countries, the character of these losses could differ substantially. Including lower-income countries in future analyses could therefore reveal stronger, but potentially more heterogeneous, effects, warranting further research tailored to those regions.

While some regions might benefit from El Niño and suffer losses during La Niña, our objective is to estimate a generalizable response to ENSO. The robustness of our results across various country-specific heterogeneities provides confidence in their global relevance, even as the underlying mechanisms and magnitudes may vary across income and climatic contexts.

## Baseline value of statistical life

The U.S. 2020 VSL estimate of USD 11.4 million used in our analysis was obtained from the U.S. Department of Health and Human Services[81], which has also been adopted in recent literature estimating economic losses associated with excess mortality and life expectancy reductions[77]. Importantly, this VSL value was not directly estimated in 2020, but rather updated from a 2013 base estimate, adjusted to 2020 U.S. dollars and income (see Ref.[81], Page D-10).

Because the original estimation predates the COVID-19 pandemic, it reflects long-term average economic and behavioral conditions rather than short-term shifts in risk perception during 2020. While minor macroeconomic adjustments from 2020 price levels are incorporated, behavioral factors such as heightened risk aversion during the pandemic are unlikely to have materially affected this benchmark.

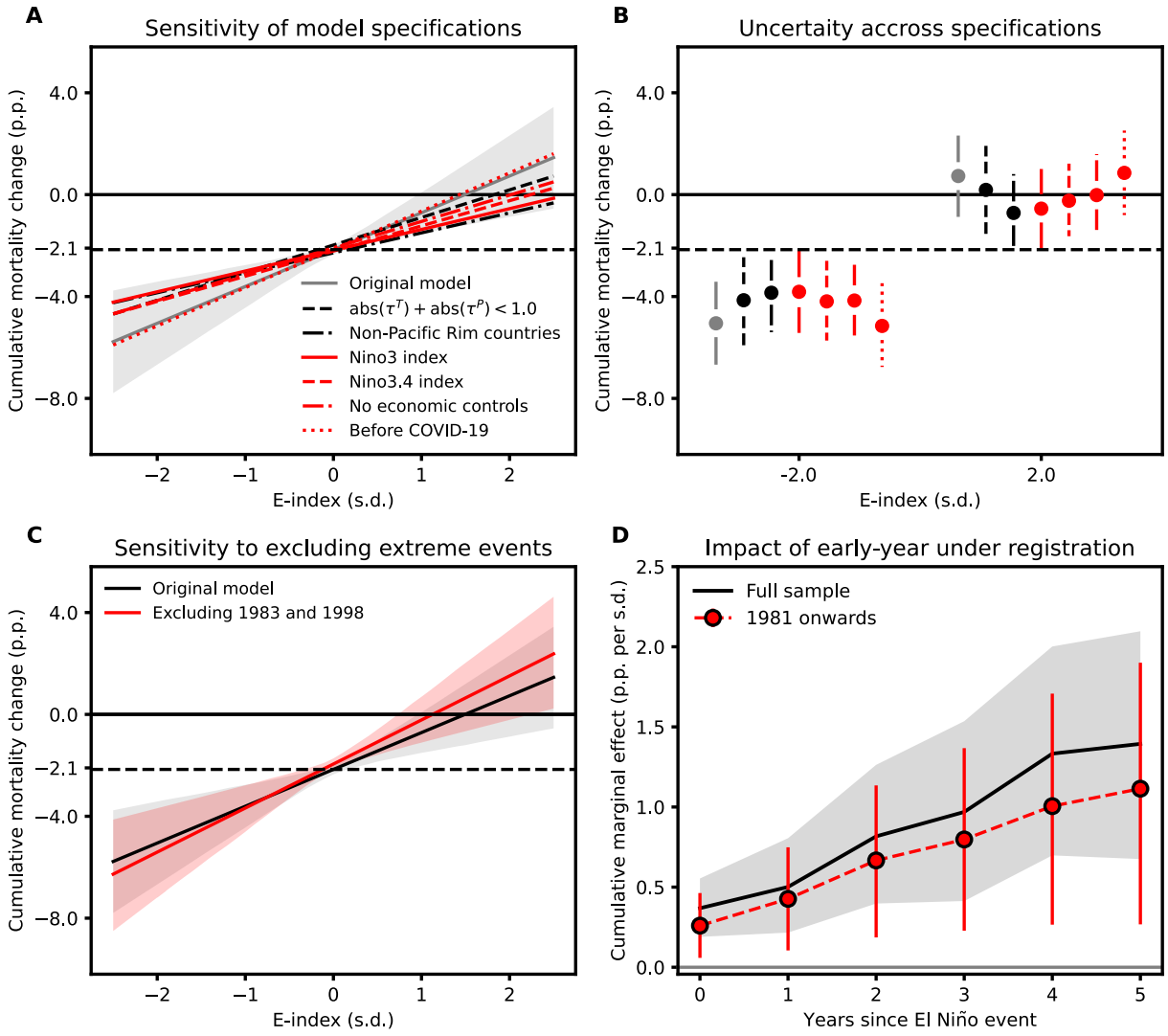



**Fig. S1. Sensitivity to model specifications.**

(**A**) 5-year cumulative mortality change across various ENSO intensity levels under different model specifications. The original model (grey line, shaded 95% CI) is compared with models excluding high teleconnection countries (black dashed), using non-Pacific Rim countries (black dot-dashed), replacing the E-index with Niño 3 (red solid) or Niño 3.4 (red dashed), removing economic controls (red dot-dashed), and excluding COVID-19 years. (**B**) Uncertainty in the 5-year cumulative mortality change (95% CI) for ENSO intensities of -2.0 and 2.0, with line styles matching (**A**). (**C**) Mortality change using the full sample (black) and excluding 1983 and 1998 (red). Solid lines show the mean, and shaded areas indicate 95% CIs from bootstrapped resampling by the country-age group. (**D**) Cumulative effect estimates from lag 0 to 5, shown for the full sample (black solid) and for the subsample excluding pre-satellite years (red dashed). The grey shaded area and red error bars indicate 95% CIs obtained from bootstrap resampling at the country-age group level for the corresponding model.

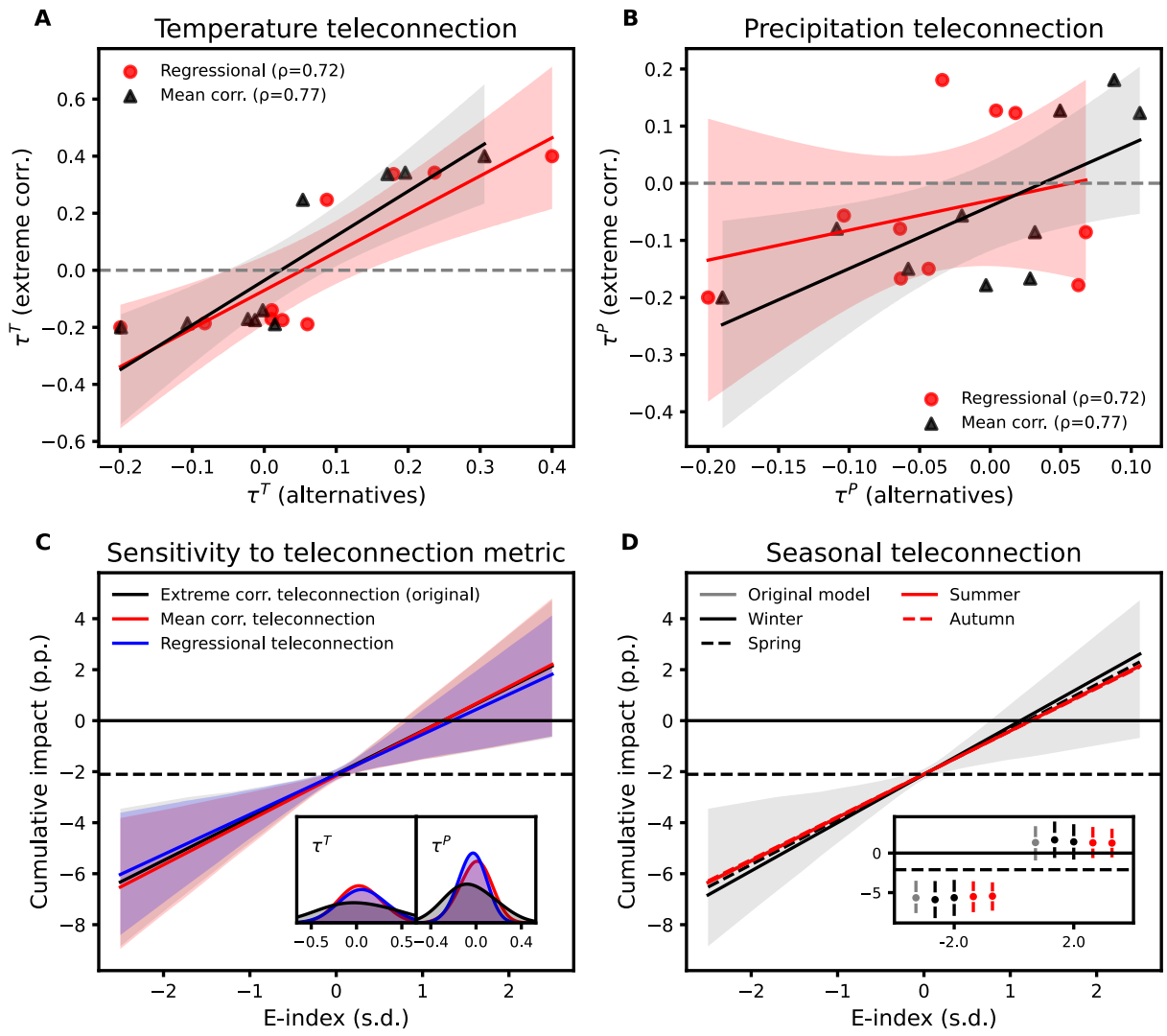



**Fig. S2. Sensitivity to teleconnection definitions.**

Comparison of alternative teleconnection measures for temperature (**A**) and precipitation (**B**). Each point represents a country-level estimate: regression-based teleconnection (red circle) and the mean correlation teleconnection (black triangle), benchmarked against the original extreme-correlation measure. Shaded bands denote 95% CIs from regression fits. Reported $\rho$ values indicate the correlation between alternative and original measures. (**C**) Sensitivity of the five-year cumulative mortality effect of ENSO intensity to the choice of teleconnection metric: the extreme-correlation measure (original, black), the regression-based measure (blue), and the mean-correlation measure (red). Shaded areas represent 95% CIs. The inset panel compares the distribution of the three teleconnection measures across countries. (**D**) Seasonal heterogeneity in teleconnection effects, contrasting cumulative mortality impacts when ENSO teleconnections are measured separately by season. Grey denotes the original model, with colored lines for winter (solid black), spring (dashed black), summer (solid red), and autumn (dashed red). The inset shows95% CIs for strong La Niña (E-index = –2) and El Niño (E-index = 2) intensities.

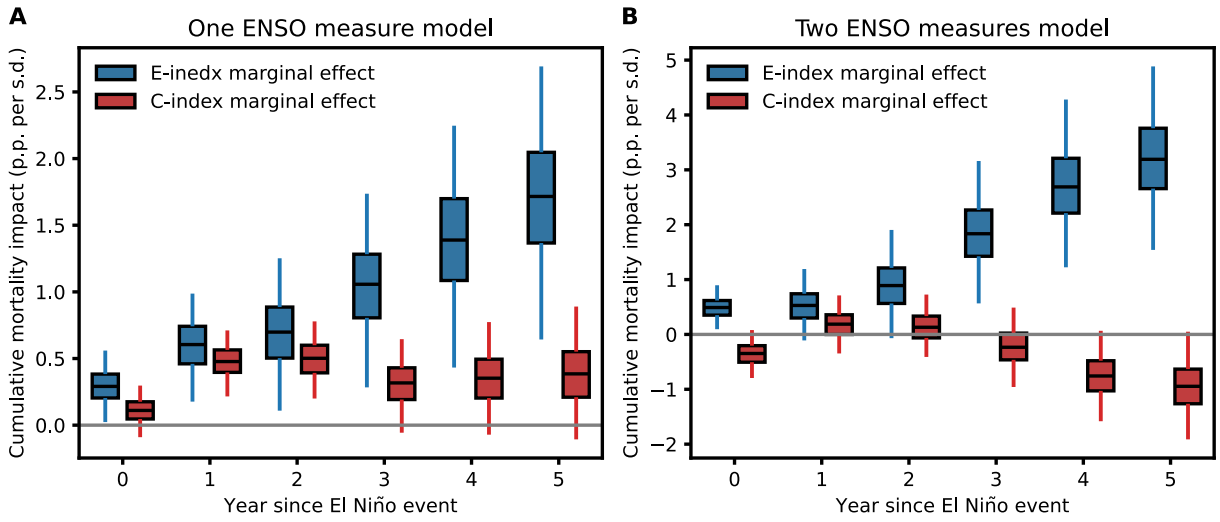



**Fig. S3. Impact of east and central Pacific ENSO.**

(**A**) Cumulative marginal impact of the E-index and C-index on mortality from lag 0 to 5 in a single ENSO measure model, where either the E-index or C-index is used as the sole measure of ENSO. (**B**) The cumulative marginal impact of the E-index and C-index on mortality from lag 0 to 5 in a two ENSO measure model, where both East and Central Pacific ENSO are considered together to assess their impact on mortality. The box indicates the interquartile range, the whisker indicates the range between the 5th and 95th percentile, and the horizontal solid line shows the median.

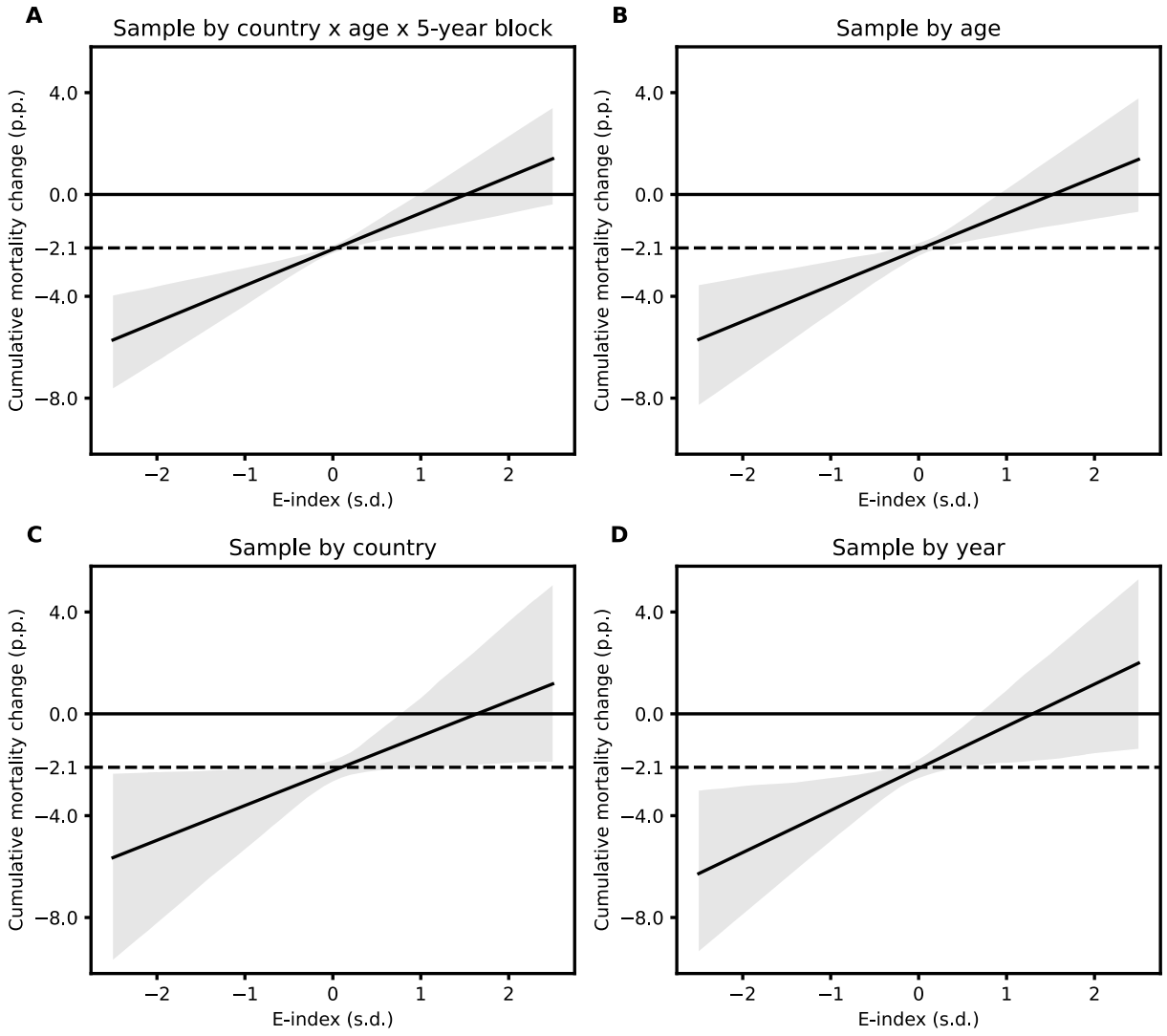



**Fig. S4. Sensitivity to bootstrapping sampling groups.**

(**A**) 5-year cumulative mortality change by ENSO intensity, with sampling based on country or region, age group, and 5-year blocks. Groups are kept intact to account for short-term temporal correlations. When ENSO intensity is 0, the mean mortality improvement is -2.1%, reflecting overall improvements across Pacific Rim countries. (**B**) Cumulative effect when sampling by age group, preserving all country-year observations within each group to account for spatial and temporal correlations. (**C**) Cumulative effects when sampling by country, keeping all age-year observations together to account for cross-age group and temporal correlations. (**D**) Cumulative effects when sampling by year, grouping all country-age observations to capture spatial and cross-age correlations. In all panels, solid lines represent the mean, shaded areas denote 95% confidence intervals, and samples are drawn from uniform distributions with replacement. Axes are consistent across panels.

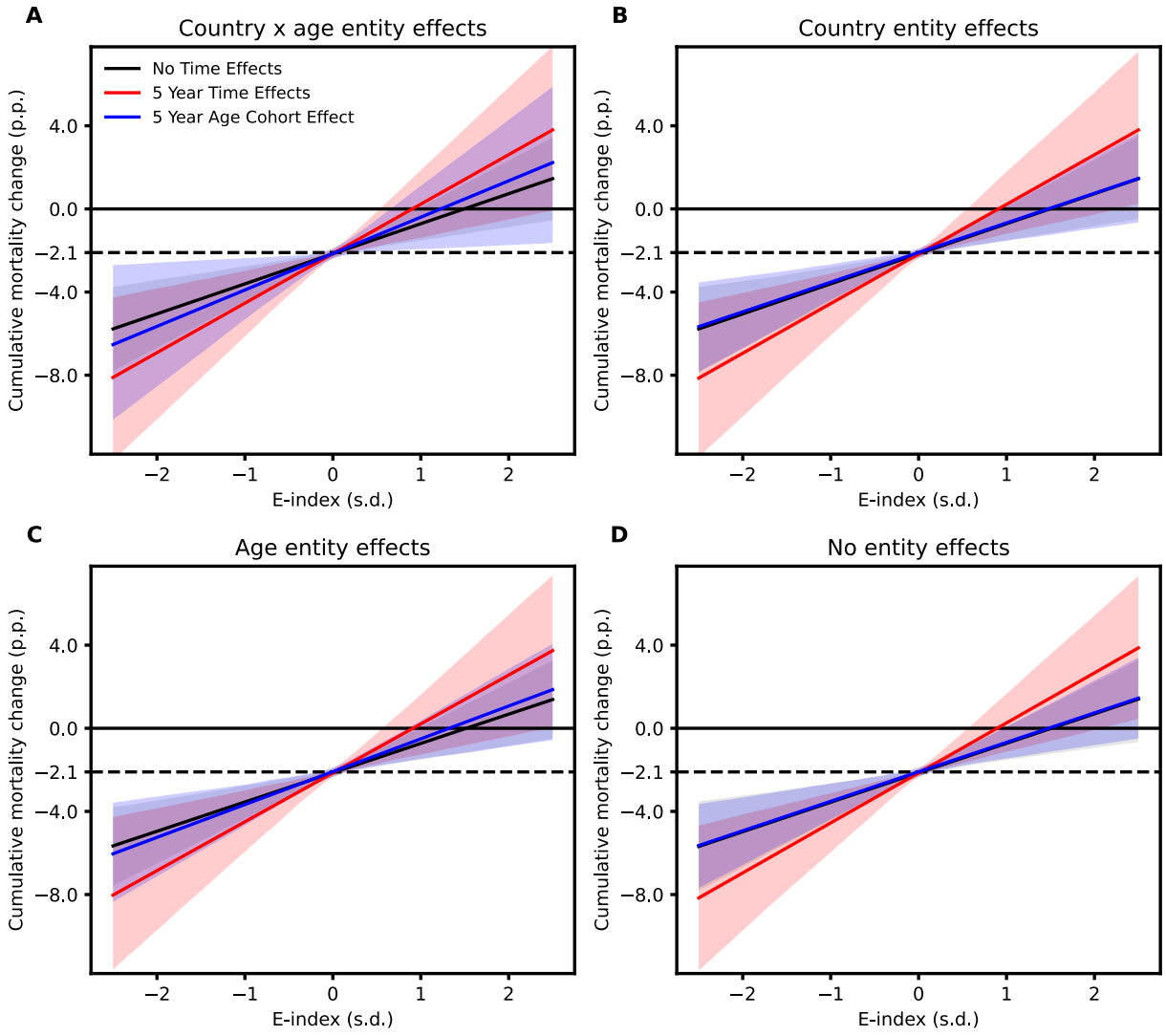



**Fig. S5. Sensitivity to fixed effects.**

(**A**) 5-year cumulative mortality change by varying levels of ENSO intensity, with the entity effect set at the country-age group level. The black line represents the cumulative mortality change by varying levels of ENSO without a time-fixed effect. The red line represents the cumulative mortality change by varying level of ENSO with the time-fixed effect set at a 5-year rolling window. The blue line represents the cumulative mortality change by varying level of ENSO when a 5-year age cohort effect is added to the model. The shaded areas, corresponding to each color, represent the 95% confidence intervals for each model. (**B** to **D**) Same as (**A**), but with the entity effect set at the country or region level, age level, and no entity effect, respectively.

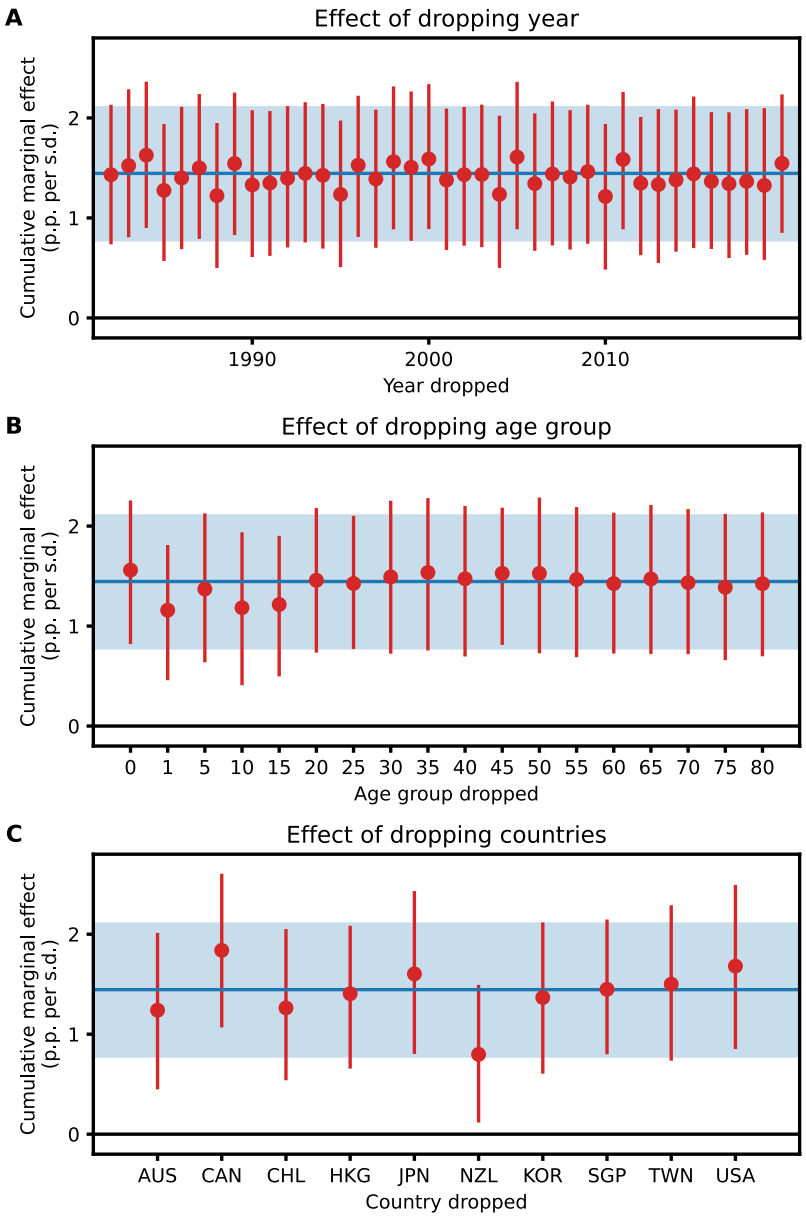



**Fig. S6. Sensitivity to treatment effects.**

5-year cumulative marginal effect of ENSO with E = 1.0 when individual years (**A**), individual age groups (**B**), and individual countries or regions (**C**) are excluded from the sample. In all panels, the solid blue line represents the marginal effect of ENSO with E = 1.0 from the original model, and the blue shaded area indicates the 95% confidence interval from the original model.

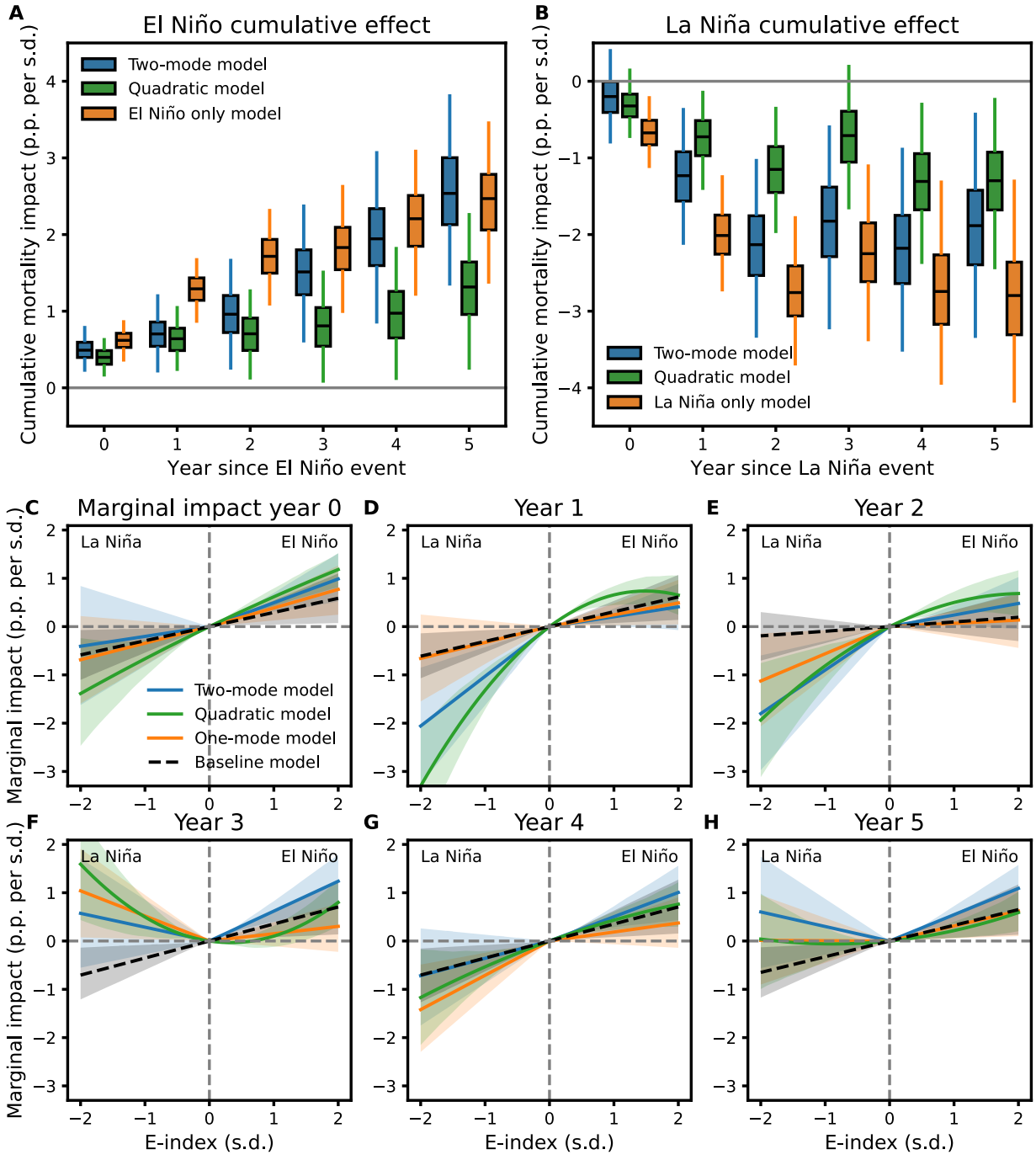



**Fig. S7. Distinct cumulative and nonlinear impacts of El Niño and La Niña events.**

Cumulative effects of El Niño (**A**) and La Niña (**B**) events on mortality improvement up to five years after onset. Results are shown for three model specifications: the two-mode model (blue), the quadratic model (green), and the single-mode model (red). Boxes indicate interquartile ranges, and whiskers represent 95% confidence intervals. (**C** to **H**) Marginal impacts of the E-index on mortality improvement by year since the ENSO event, from year 0 to year 5. Lines show model-estimated marginal effects from the two-mode (blue), quadratic (green), and one-mode (red) specifications, with the baseline model in black dashed for comparison. Shaded bands denote 95% CIs from bootstrap resampling.

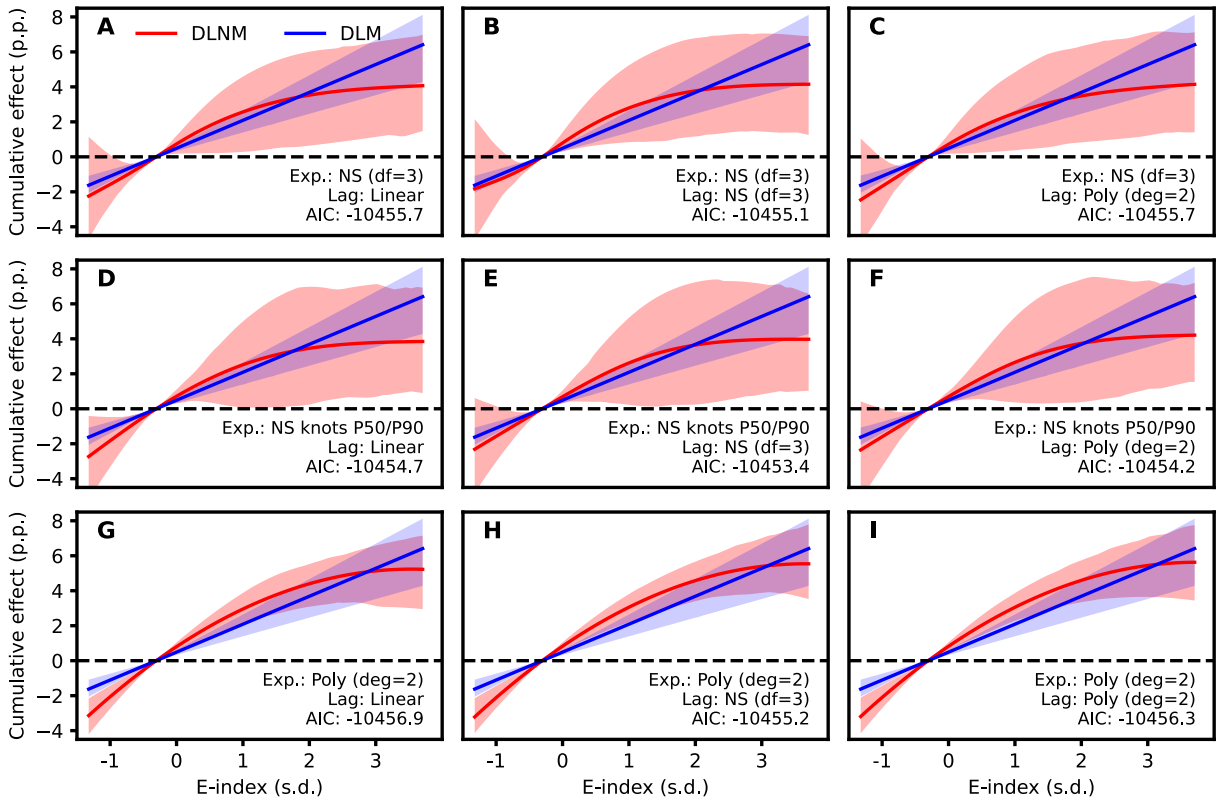



**Fig. S8. Five-year cumulative effect of ENSO under alternative distributed lag nonlinear model specifications.**

(**A** to **I**) Compare estimates of the five-year cumulative impact of the ENSO E-index on mortality improvement across different distributed lag structures and exposure–response forms. Red lines show distributed lag nonlinear model (DLNM) estimates and blue lines the simpler distributed lag model (DLM), with shaded areas denoting 95% CIs. The exposure term (Exp.), lag term (Lag), and AIC values of each specification are reported in each subfigure.

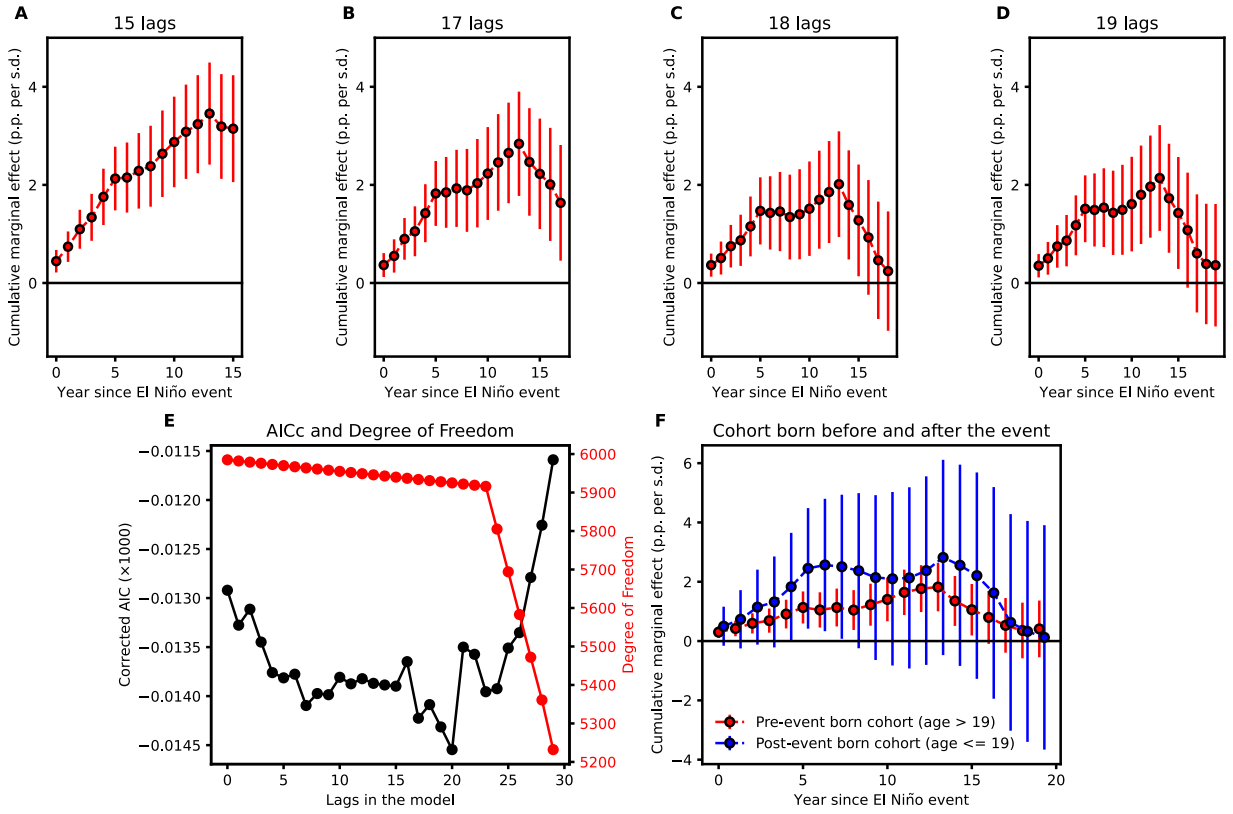



**Fig. S9. Sensitivity of main regression result to additional lags.**

(**A** to **D**) Regression results estimated with 15 (**A**), 17 (**B**), 18 (**C**), and 19 (**D**) lags in the model. Confidence intervals are estimated through bootstrap resampling, as in the main analysis. (**E**) The black line shows the Corrected Akaike Information Criterion (AICc) values for regression models with increasing lags from 0 to 29, where lower AICc values are more desirable. The red line indicates the degrees of freedom for the same set of models. (**F**) Regression results for separate samples: the red line represents the cumulative marginal effect of 19 lags in the model for the cohort born before the ENSO events, while the blue line represents the cumulative marginal effect of 19 lags for the cohort born after the ENSO events.

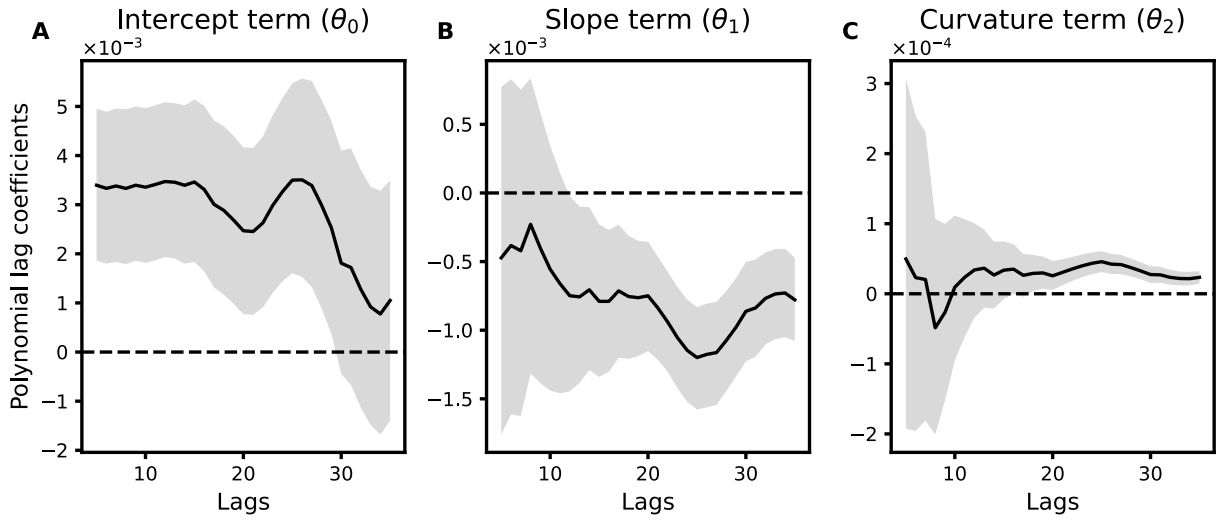



**Fig. S10. Polynomial distributed lag model coefficients (order 2) across additional lags.**

Estimated lag coefficients from the polynomial distributed lag model of order two, for up to 40 lags. (**A**) intercept term ($\theta_0$), (**B**) slope term ($\theta_1$), and (**C**) curvature term ($\theta_2$). Solid lines represent point estimates, and shaded areas denote the 95% CIs obtained from bootstrapped resampling.

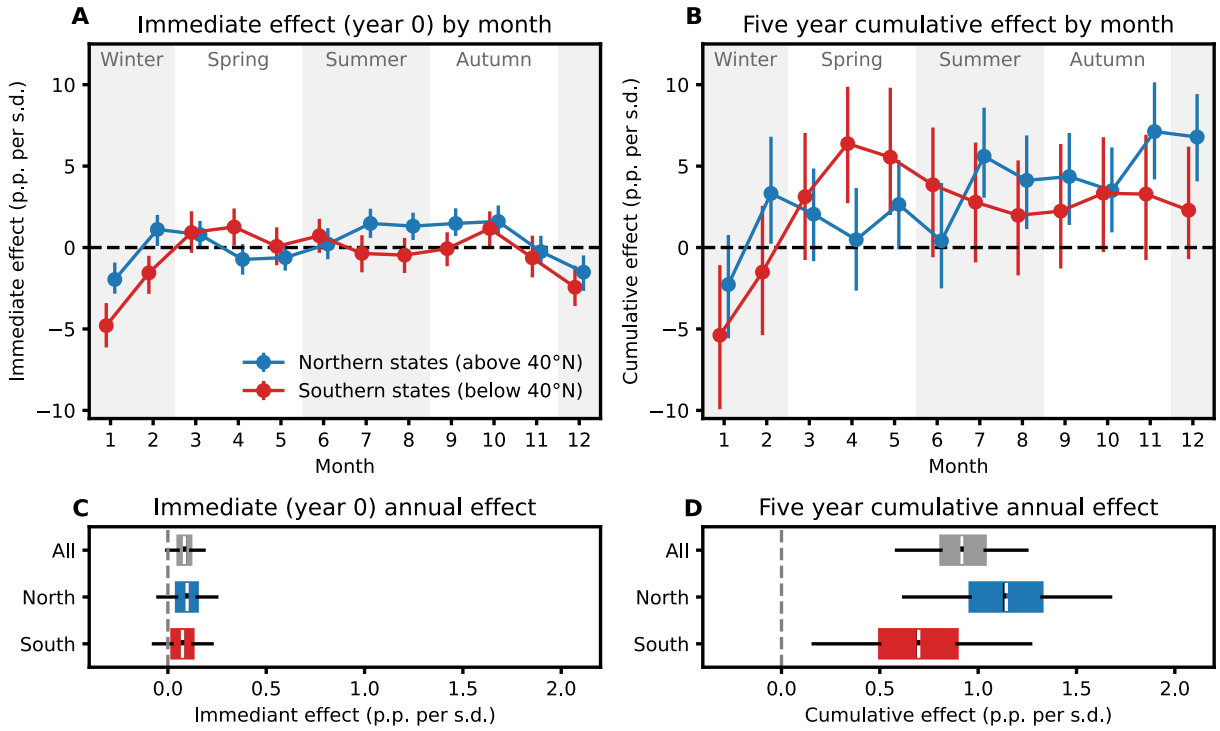



**Fig. S11. Monthly and annual effects of ENSO on U.S. mortality improvements.**

(**A**, **B**) present impacts on monthly mortality improvement, contrasting northern continental states (blue, above 40°N) and southern continental states (red, below 40°N). (**A**) The immediate effect at the onset year (year 0). (**B**) shows the five-year cumulative effect for each month since ENSO onset. Shaded vertical bands mark climatological seasons (winter, spring, summer, autumn). (**C**, **D**) summarize the impacts on annual mortality improvement, with boxes indicating interquartile ranges, whiskers showing 95% CIs, solid black lines for medians, and white dashed lines for means. (**C**) The annual immediate effect in year 0. (**D**) shows the annual cumulative effect over five years.

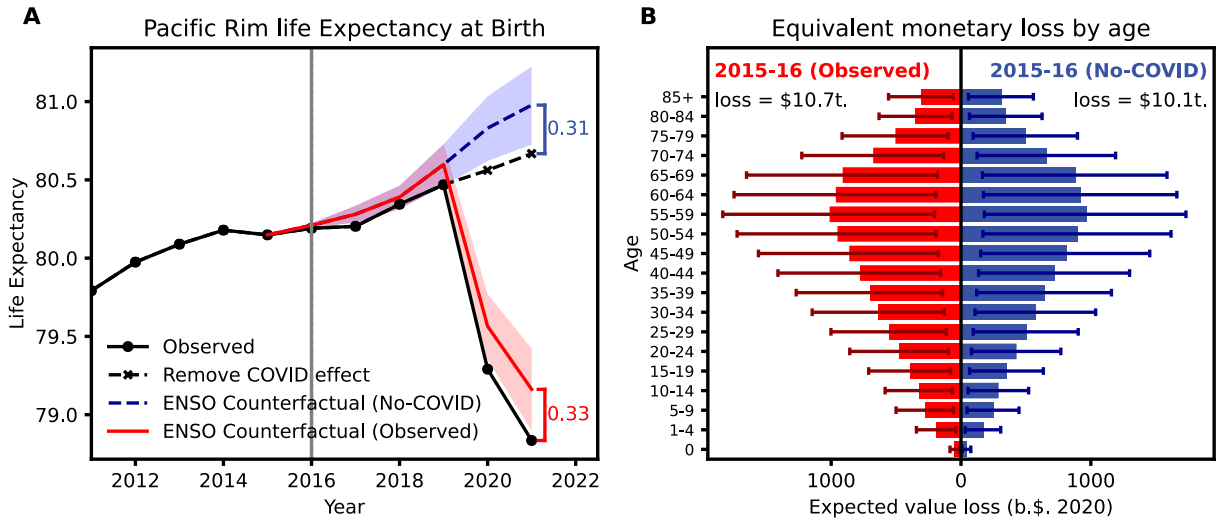



**Fig. S12. Pacific Rim life expectancy and economic losses associated with 2015-16 El Niño.**

(**A**) Life expectancy at birth around the 2015–2016 El Niño event under different scenarios. The observed trajectory (solid black) is compared with three counterfactuals: removes the estimated COVID-19 effect (dashed black), the ENSO counterfactual without COVID-19 (dashed blue), and the ENSO counterfactual including COVID-19 (dashed red). Shaded areas indicate 95% confidence intervals from bootstrap resampling by country–age group. (**B**) Equivalent monetary loss by age group for the 2015–16 El Niño, comparing observed outcomes (red) with the no-COVID counterfactual (blue). Bars represent expected value losses in 2020 US dollars, with horizontal lines denoting 95% CIs.

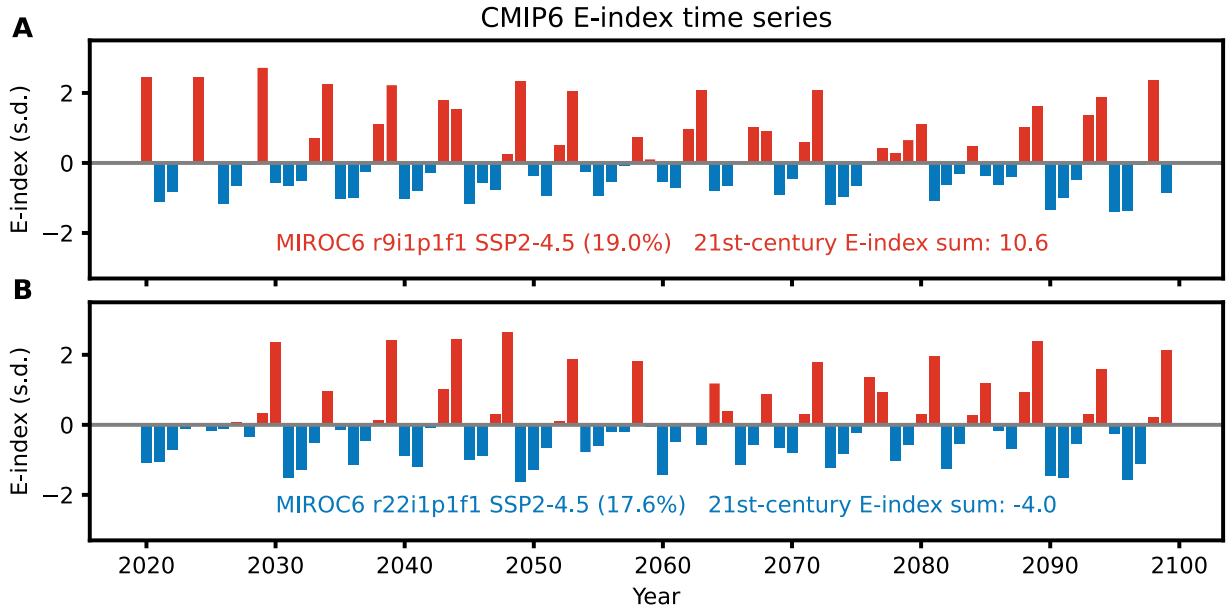



**Fig. S13. CMIP6 E-index time series example.**

(**A–B**) The E-index time series from two example simulations are presented, each representing simulations with similar amplitude changes and volatility but markedly different 21st-century E-index sums. The top panel displays MIROC6 r9i1p1f1 from the SSP2-4.5 experiment, while the bottom panel shows MIROC6 r22i1p1f1 from the same SSP2-4.5 experiment. Red bars indicate eastern Pacific El Niño events (E-index $\geq 0$), and blue bars indicate eastern Pacific La Niña events (E-index $< 0$). The left inset in each panel provides model details and the amplitude change, while the right inset shows the sum of the E-index for the 21st century. Positive sums indicate more El Niño events than La Niña events, and negative sums indicate the opposite.

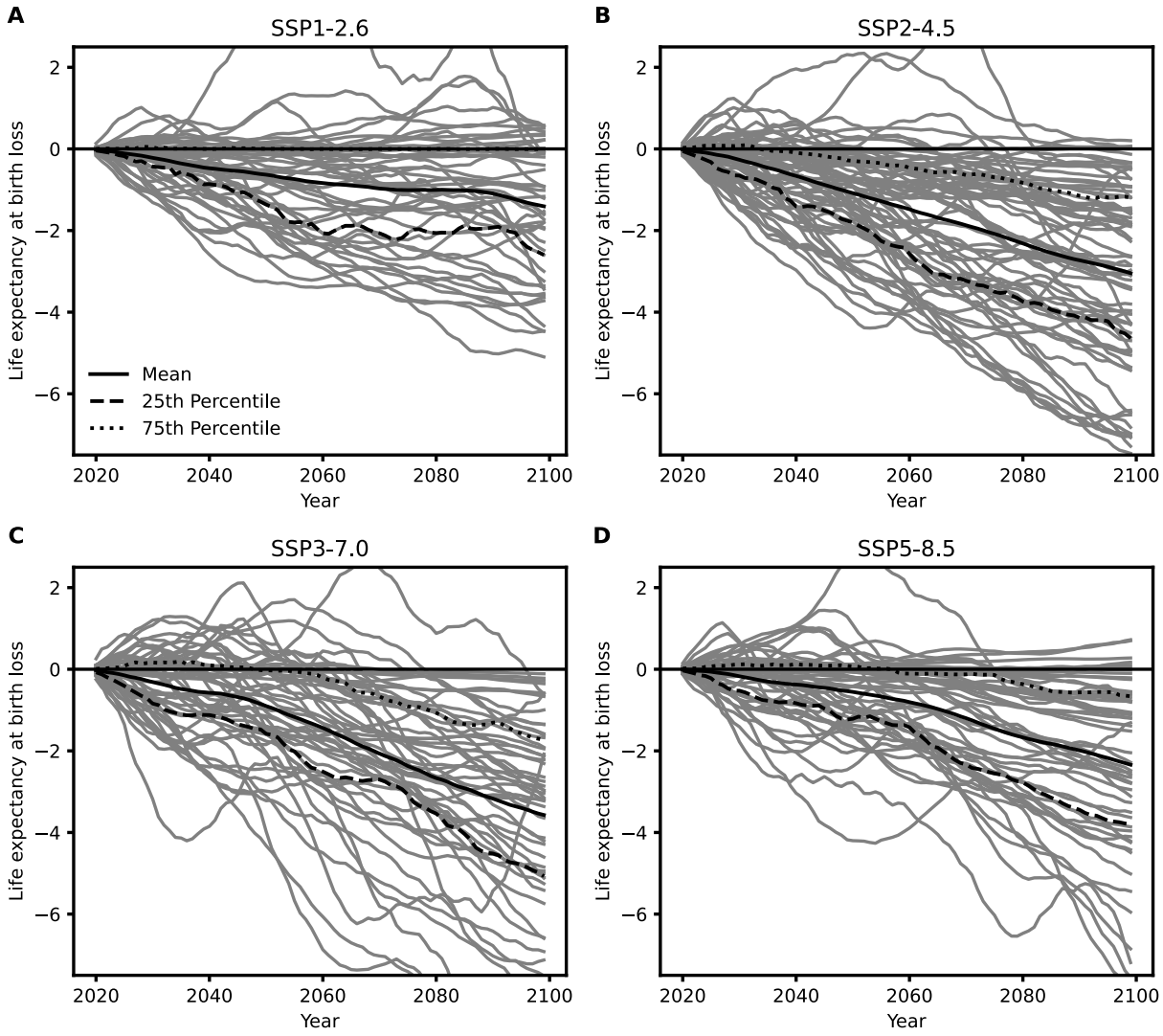



**Fig. S14. Projected life expectancy loss from ENSO time-series.**

(**A** to **D**) Projected life expectancy loss at birth due to ENSO for each simulation across the four SSP experiments. In each panel, grey lines represent the time series for individual simulations, while the solid black line shows the mean life expectancy loss for that year. The dashed black line and dotted black line indicate the 25th and 75th percentiles, respectively. Negative value suggests a slowdown in life expectancy improvement as a result of ENSO's impact.

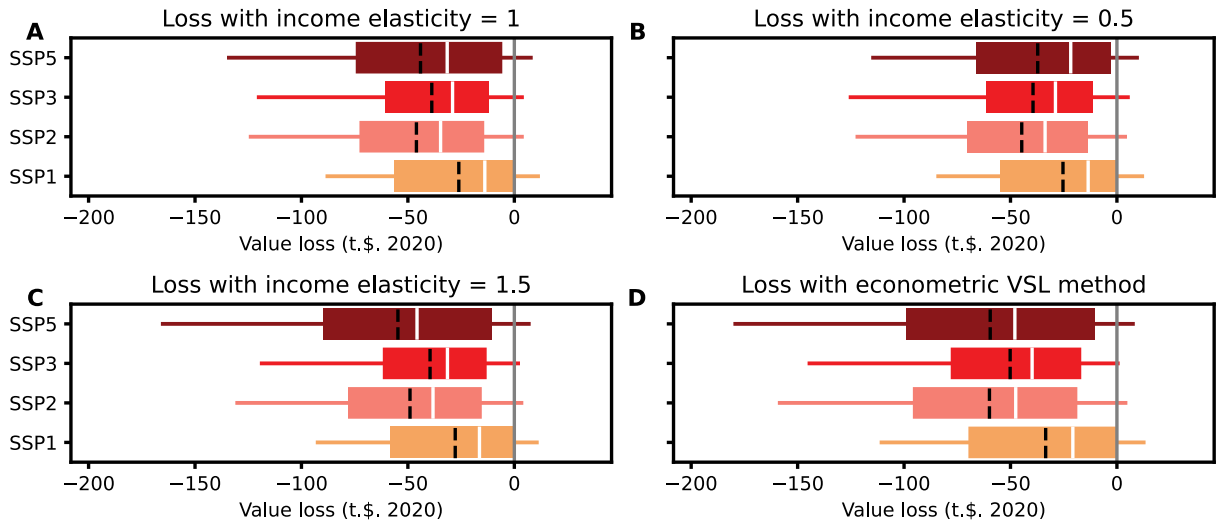



**Fig. S15. Mortality value loss projection by VSL methods.**

(**A** to **C**) Mortality value loss projections by SSP scenarios using the value of statistical life estimated with the income reference method, with income elasticity set to 1, 0.5, and 1.5. (**D**) Mortality value loss projections by SSP scenarios using the value of statistical life estimated with the formula method.

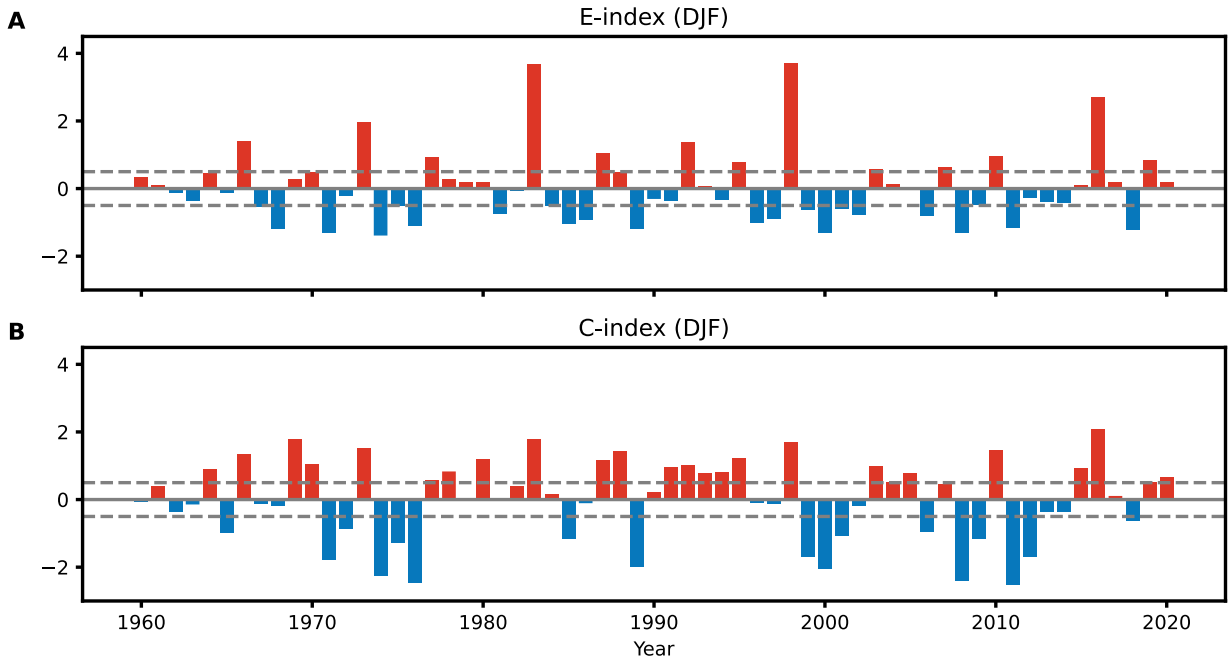



**Fig. S16. Interannual E and C indices.**

(**A**) E-index during December-January-February season. (**B**) C-index during December-January-February (DJF) season.

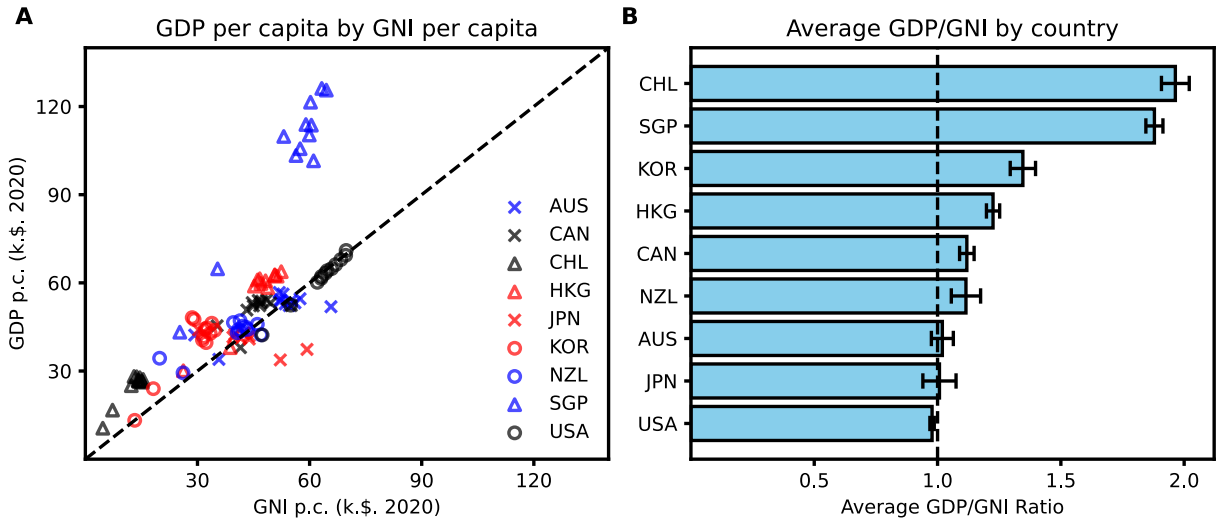



**Fig. S17. Gross domestic product and gross national income relation.**

(**A**) Gross domestic product per capita versus gross national income per capita by country, measured in 2020 dollars. (**B**) Ratio of gross domestic product to gross national income by country. Bars represent the mean, and error bars indicate the 95% confidence intervals.

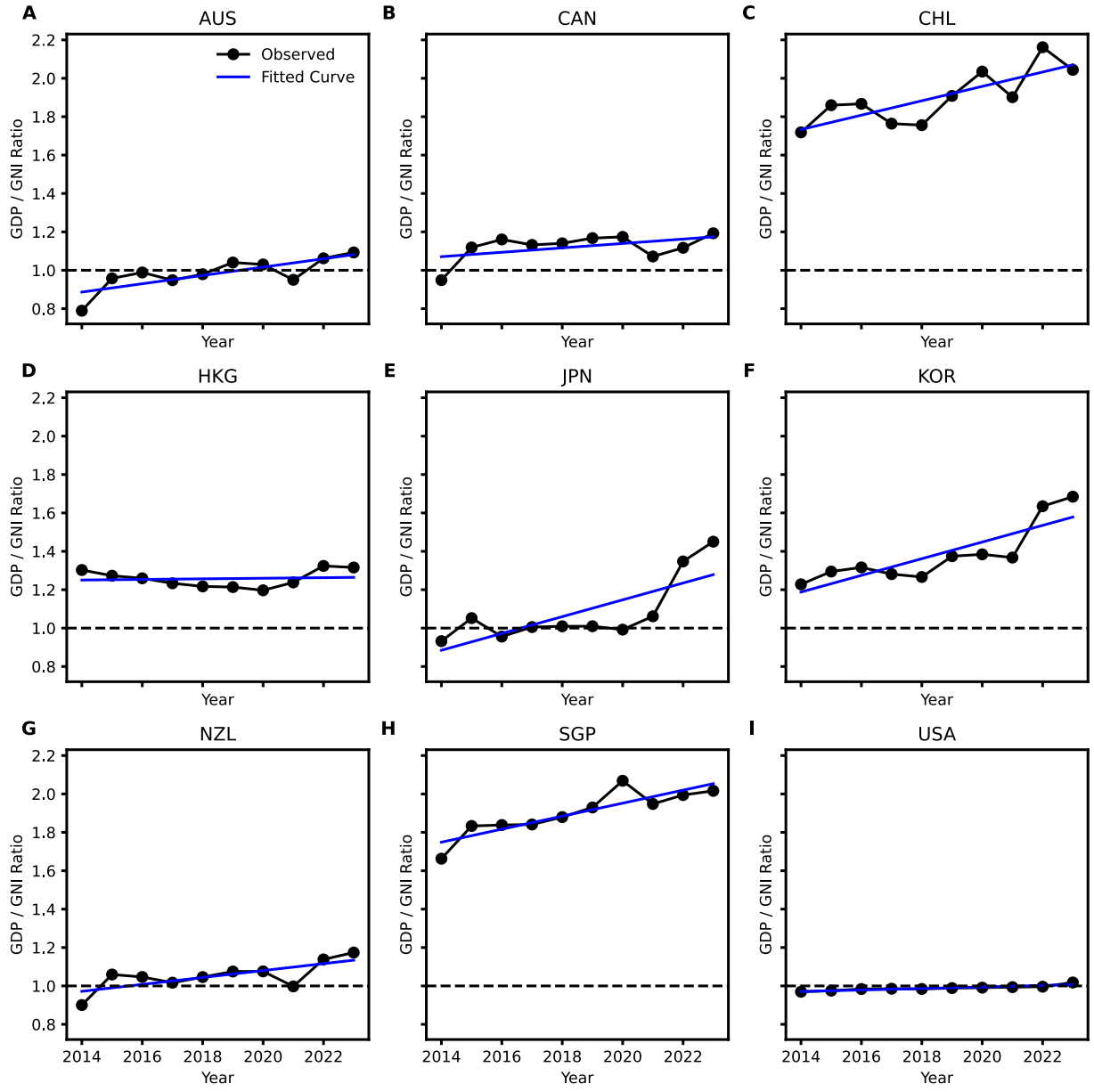



**Fig. S18. Gross domestic product by gross national income relation by countries and regions.**

The countries and regions included in the analysis are Australia (AUS), Canada (CAN), Chile (CHL), Hong Kong SAR (HKG), Japan (JPN), South Korea (KOR), New Zealand (NZL), Singapore (SGP), and the United States (USA).

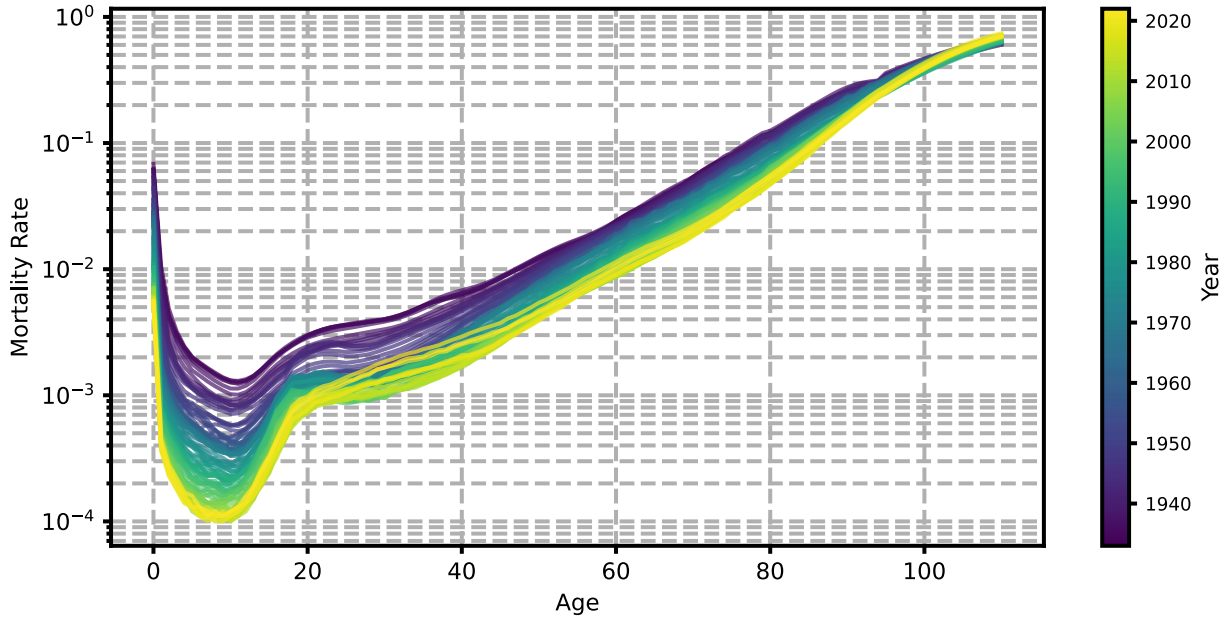



**Fig. S19. US mortality curve: An example.**

Each line represents a different year, with colors transitioning from blue to yellow (1933 to 2022).

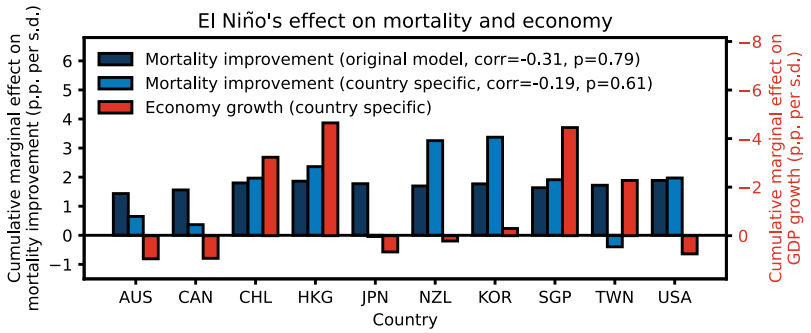



**Fig. S20. ENSO impact on mortality improvement and economic growth by each country.**

The cumulative 5-year marginal impact of ENSO on mortality changes (blue) and economic growth (measured by GDP growth, red) for each country. Adverse impacts are indicated by positive shifts in mortality and negative shifts in economic growth.

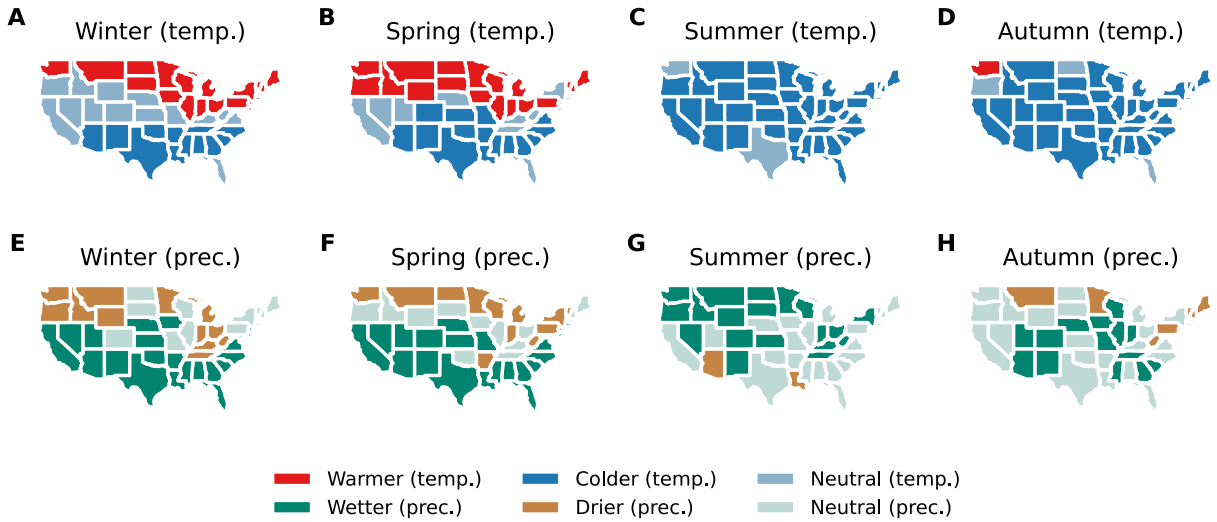



**Fig. S21. Seasonal teleconnections with the continental U.S.**

(**A** to **D**) show the seasonal ENSO temperature teleconnections, with red indicating states that are significantly warmer during El Niño years, blue indicating colder states, and light blue denoting neutral responses. (**E** to **H**) show the seasonal ENSO precipitation teleconnections, with green indicating wetter states, brown indicating drier states, and grey indicating neutral responses.

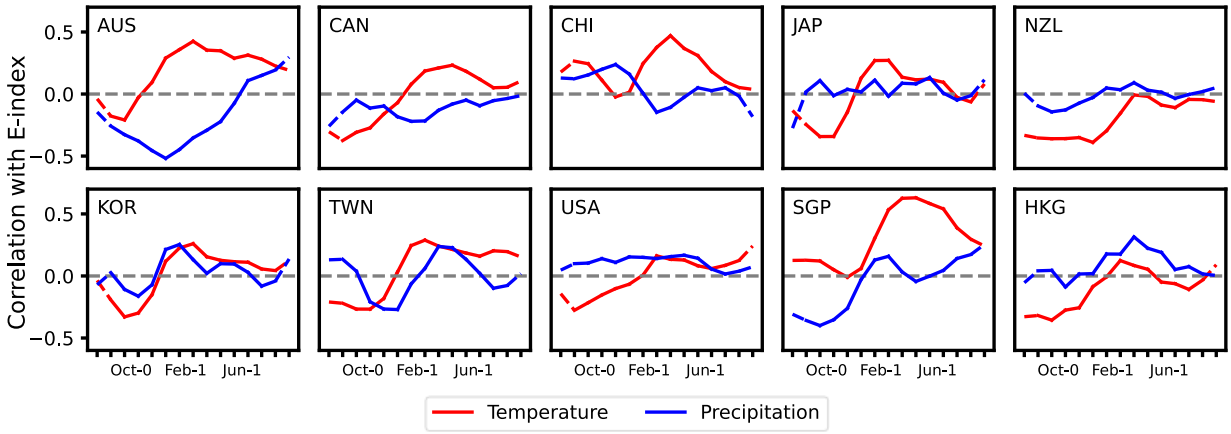



**Fig. S22. Monthly teleconnection by country in the Pacific Rim.**

Monthly teleconnection profiles by country, showing 3-month rolling correlation between the ENSO E-index and local climate anomalies: temperature teleconnections ($\tau^T$, red) and precipitation teleconnections ($\tau^P$, blue).

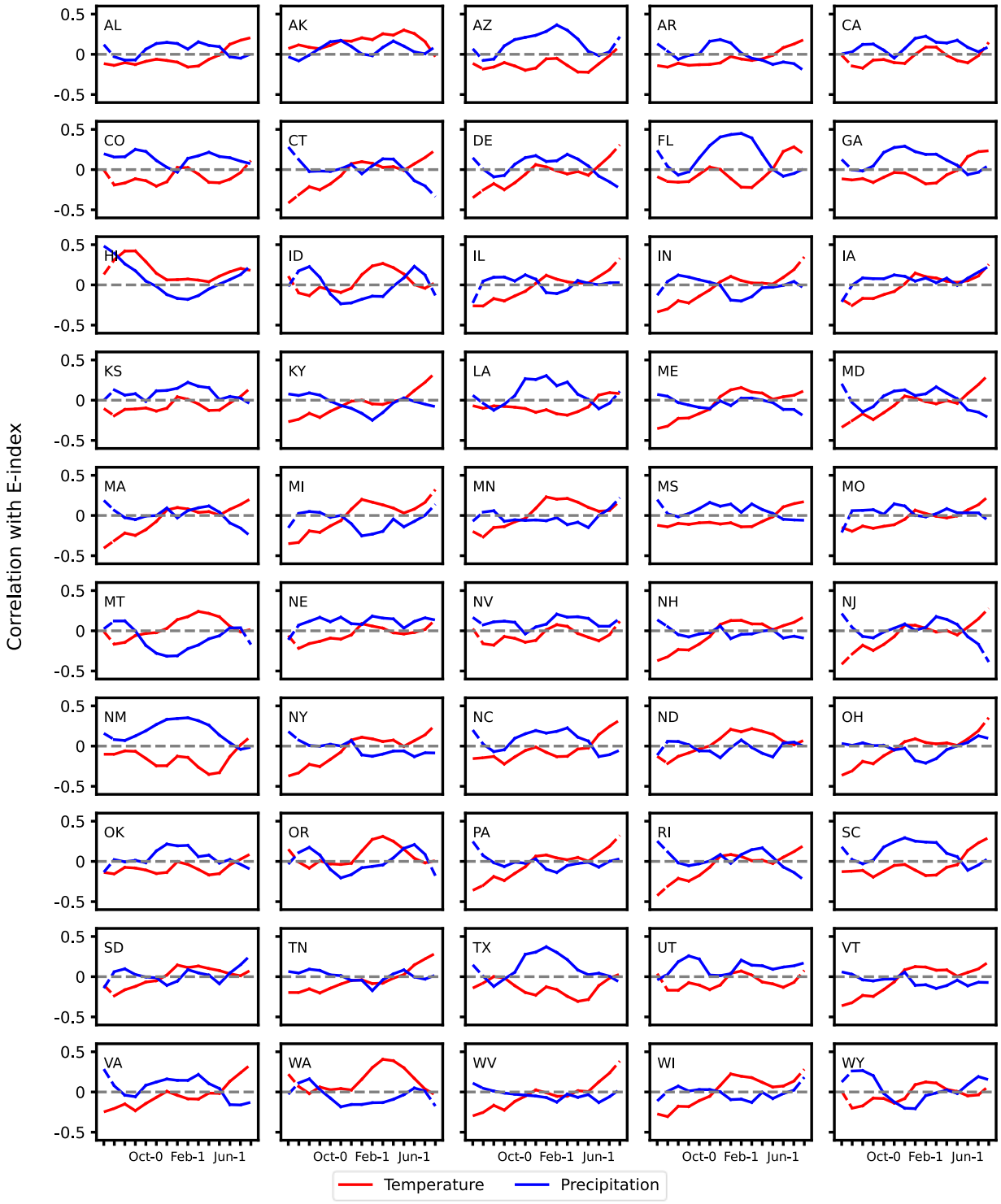



**Fig. S23. Monthly teleconnection by state in the U.S.**

Monthly teleconnection profiles by state, showing 3-month rolling correlation between the ENSO E-index and local climate anomalies: temperature teleconnections ($\tau^T$, red) and precipitation teleconnections ($\tau^P$, blue).

**Table S1. Two-Stage Least Squares Test on E-index Endogeneity.**

This table presents the Two-Stage Least Squares (2SLS) test for potential endogeneity of the E-index, using the Sea Level Pressure (SLP) index as an instrument. The SLP index is derived from standardized principal components of SLP data over the Pacific Ocean (1º×1º grid) from March to May (MAM) of year *t*-1, ensuring no overlap with ENSO formation. Panel A reports first-stage results, confirming the SLP index as a strong instrument (p = 0.007, Cragg-Donald test). Panel B presents second-stage results, replicating column (1) from Table S8, showing that the 2SLS estimates remain robust, with coefficients of similar magnitude. All values represent estimated coefficients, with t-statistics in parentheses. "***" indicates a *p*-value < 0.01, "**" signifies a *p*-value < 0.05, and "*" denotes a *p*-value < 0.1. The overidentification test ($p$ = 1.000) suggests instrument validity.

| Panel A: First Stage, Endogenous Variable: $E_t$ | |
|---|---|
| SP-index | 0.79*** |
| | (2.80) |
| Constant | 0.84 |
| | (-0.21) |
| Observations | 60 |
| First-stage Cragg and Donald test | (p-value=0.007) |

| Panel B: Second Stage, Dependent Variable: Mortality Improvement Rate | | | |
|---|---|---|---|
| | $E_{t-h}$ | $E_{t-h} \times \tau^T$ | $E_{t-h} \times \tau^P$ |
| | (1) | (2) | (3) |
| *h* (lags) | | | |
| 0 | 0.70** | 0.25 | 1.17 |
| | (2.02) | (0.37) | (1.26) |
| 1 | 1.10*** | 0.76* | -0.10 |
| | (3.72) | (1.36) | (-0.13) |
| 2 | 0.09 | -0.08 | -1.83*** |
| | (0.28) | (-0.14) | (-2.49) |
| 3 | -0.23 | 0.53 | 0.44 |
| | (-0.71) | (0.91) | (0.59) |
| 4 | 0.18 | -0.57 | 0.28 |
| | (0.56) | (-0.90) | (0.32) |
| 5 | 0.85*** | 0.59 | 0.95 |
| | (2.63) | (0.96) | (1.26) |
| Control variables | | | Yes |
| Country and Age fixed effect | | | Yes |
| Observations | | | 5,814 |
| Overidentification test | | | (p-value=1.000) |

## Table S2. Causal Chain from ENSO to Mortality Improvement

This table reports tests of the causal chain linking ENSO to mortality improvement under a structural causal model through three health-stress mechanisms (health expenditure, air pollution, and heat extremes), comparing the immediate effect at $t$=0, with the cumulative effect from $t$=0 to 5. Panel A and Panel B present the mediator model and the outcome model, with statistical significance assessed by two-sided tests. Panel C reports the indirect, direct, and total effects, with significance assessed by one-sided tests. Panel D shows the distribution of the mediated share across bootstrap replications. The displayed values represent the estimated coefficients for each variable, with t-statistics reported in parentheses below. "***" indicates a $p$-value < 0.01, "**" signifies a $p$-value < 0.05, and "*" denotes a $p$-value < 0.1.

| *Heath-stress mechanisms:* | Health expenditure | | Air pollution (PM2.5) | | Heat extremes (TXx) | |
|---|---|---|---|---|---|---|
| | Immediate | Cumulative | Immediate | Cumulative | Immediate | Cumulative |
| | (1) | (2) | (3) | (4) | (5) | (6) |
| *Panel A: Stage 1 mediator model* | | | | | | |
| E-index (a) | 0.59*** | -2.56*** | -0.25 | 3.35** | 9.03*** | 4.17 |
| | (10.62) | (-10.07) | (-1.36) | (2.58) | (8.49) | (0.60) |
| *Panel B: Stage 2 outcome model* | | | | | | |
| Mediator (b) | -5.59*** | -5.85** | 7.33** | 5.97* | 0.35*** | 0.45*** |
| | (-2.70) | (-2.58) | (1.98) | (1.66) | (3.08) | (4.10) |
| E-index (c) | 0.32*** | 1.27*** | -0.08 | 2.79** | 0.17* | 1.59*** |
| | (3.59) | (2.92) | (-0.38) | (2.48) | (1.73) | (3.75) |
| *Panel C: Causal summary* | | | | | | |
| Mediation effect (a × b) | -0.03*** | 0.15*** | -0.02 | 0.20* | 0.03*** | 0.02 |
| | (-2.64) | (2.52) | (-1.07) | (1.36) | (2.81) | (0.60) |
| Direct effect (c) | 0.32*** | 1.27*** | -0.08 | 2.79*** | 0.17** | 1.59*** |
| | (3.59) | (2.92) | (-0.38) | (2.48) | (1.73) | (3.75) |
| Total effect (c + a × b) | 0.29*** | 1.42*** | -0.10 | 3.00*** | 0.21** | 1.61*** |
| | (3.24) | (3.30) | (-0.47) | (2.56) | (2.06) | (3.76) |
| *Panel D: Share mediated* | | | | | | |
| Median | -11.6% | 10.4% | 4.1% | 6.1% | 14.6% | 1.3% |
| Inter-Quartile | [-16.1%, -8.1%] | [7.3%, 14.1%] | [-4.1%, 14.4%] | [3.5%, 9.0%] | [9.8%, 22.5%] | [0.1%, 2.2%] |
| [90% CI] | [-26.6%, -4.3%] | [3.5%, 25.3%] | [-92.8%, 74.4%] | [0.2%, 17.7%] | [4.2%, 62.2%] | [-2.9%, 4.7%] |
| [95% CI] | [-32.6%, -3.1%] | [2.4%, 29.2%] | [-275%, 118%] | [-2.7%, 20.7%] | [-17.0%, 99.6%] | [-3.8%, 6.0%] |
| Country and age fixed effect | Yes | | Yes | | Yes | |
| Sample period | 1983-2019 | | 2011-2019 | | 1982-2019 | |
| Observations | 5,706 | | 882 | | 4,788 | |

## Table S3. Country-specific Value of Statistical Life and Loss

Panels A and B report the estimated country level value of statistical life (VSL) in million dollars and corresponding economic losses in billion dollars, with 95% confidence intervals in brackets, for the 1982–83 and 1997–98 El Niño events, respectively. Columns represent alternative income elasticity assumptions (0.5, 1.0, and 1.5) applied to adjust the base U.S. VSL according to each country's per-capita income level.

Panel A: 1982-83 event

| | Income elasticity = 0.5 | | Income elasticity = 1.0 | | Income elasticity = 1.5 | |
|---|---|---|---|---|---|---|
| Country | VSL (m.) | Value loss (b.) | VSL (m.) | Value loss (b.) | VSL (m.) | Value loss (b.) |
| USA | 5.41 | 4,408 [1,393, 7,375] | 2.57 | 2,093 [662, 3,502] | 1.22 | 994 [314, 1,663] |
| JPN | 4.56 | 780 [274, 1,286] | 1.83 | 312 [110, 515] | 0.73 | 125 [44, 206] |
| CAN | 4.95 | 205 [89, 322] | 2.15 | 89 [39, 140] | 0.93 | 39 [17, 61] |
| TWN | 2.41 | 54 [19, 86] | 0.51 | 11 [4, 18] | 0.11 | 2 [1, 4] |
| AUS | 4.82 | 82 [-4, 163] | 2.04 | 35 [-2, 69] | 0.86 | 15 [-1, 29] |
| NZL | 3.85 | 24 [13, 35] | 1.3 | 8 [4, 12] | 0.44 | 3 [1, 4] |
| KOR | 2.09 | 106 [-109, 320] | 0.38 | 19 [-20, 59] | 0.07 | 4 [-4, 11] |
| CHL | 1.82 | 66 [-53, 180] | 0.29 | 11 [-8, 29] | 0.05 | 2 [-1, 5] |
| HKG | 3.44 | 51 [13, 88] | 1.04 | 15 [4, 27] | 0.31 | 5 [1, 8] |
| SGP | 3.52 | 20 [-12, 52] | 1.09 | 6 [-4, 16] | 0.34 | 2 [-1, 5] |

Panel B: 1997-98 event

| | Income elasticity = 0.5 | | Income elasticity = 1.0 | | Income elasticity = 1.5 | |
|---|---|---|---|---|---|---|
| Country | VSL (m.) | Value loss (b.) | VSL (m.) | Value loss (b.) | VSL (m.) | Value loss (b.) |
| USA | 8.03 | 5,167 [1,763, 8,561] | 5.65 | 3,639 [1,241, 6,028] | 3.98 | 2,562 [874, 4,245] |
| JPN | 8.39 | 780 [274, 1,286] | 6.18 | 692 [173, 1,243] | 4.55 | 509 [127, 915] |
| CAN | 6.48 | 205 [89, 322] | 3.69 | 103 [36, 173] | 2.1 | 58 [21, 99] |
| TWN | 5.43 | 54 [19, 86] | 2.59 | 31 [3, 56] | 1.23 | 14 [1, 25] |
| AUS | 6.64 | 82 [-4, 163] | 3.87 | 31 [-17, 76] | 2.25 | 18 [-10, 45] |
| HKG | 7.11 | 51 [13, 88] | 4.43 | 58 [17, 99] | 2.76 | 36 [11, 62] |
| NZL | 5.64 | 24 [13, 35] | 2.79 | 10 [5, 16] | 1.38 | 5 [2, 8] |
| KOR | 4.56 | 106 [-109, 320] | 1.82 | 40 [-84, 168] | 0.73 | 16 [-34, 67] |
| CHL | 3.32 | 66 [-53, 180] | 0.96 | 31 [-22, 81] | 0.28 | 9 [-6, 23] |
| SGP | 6.95 | 20 [-12, 52] | 4.24 | 21 [-20, 62] | 2.58 | 13 [-12, 38] |

**Table S4. ENSO Measures Lag Multicollinearity Test.**

This table presents two multicollinearity tests for the ENSO lags. Columns (1) to (6) present the E-index lag correlations up to 5 lags, as well as the correlation of each E-index lag with the C-index. Column (7) presents the variance inflation factor (VIF) test.

| | Correlation test | | | | | | VIF test |
|---|---|---|---|---|---|---|---|
| Lag variable | $E_{t-1}$ | $E_{t-2}$ | $E_{t-3}$ | $E_{t-4}$ | $E_{t-5}$ | $C_t$ | VIF |
| | (1) | (2) | (3) | (4) | (5) | (6) | (7) |
| $E_t$ | -0.164 | -0.367 | 0.039 | 0.056 | 0.058 | 0.760 | 1.28 |
| $E_{t-1}$ | | -0.167 | -0.368 | 0.039 | 0.052 | -0.132 | 1.40 |
| $E_{t-2}$ | | | -0.154 | -0.372 | 0.005 | -0.341 | 1.70 |
| $E_{t-3}$ | | | | -0.153 | -0.347 | 0.099 | 1.65 |
| $E_{t-4}$ | | | | | -0.170 | 0.119 | 1.40 |
| $E_{t-5}$ | | | | | | 0.094 | 1.27 |

**Table S5. Linear Trend of PPP-to-GNI Ratio by Country and Region.**

This table presents the trend of the PPP-to-GNI ratio by countries and regions. Columns (1) and (2) display the coefficients for the year and constant, with t-statistics reported in parentheses below. "***" indicates a *p*-value < 0.01, "**" signifies a *p*-value < 0.05, and "*" denotes a *p*-value < 0.1. Column (3) reports the R-squared value from the country-level regression. The countries and regions included in the analysis are Australia (AUS), Canada (CAN), Chile (CHL), Hong Kong SAR (HKG), Japan (JPN), South Korea (KOR), New Zealand (NZL), Singapore (SGP), and the United States (USA).

| | AUS | CAN | CHL | HKG | JPN | KOR | NZL | SGP | USA |
|---|---|---|---|---|---|---|---|---|---|
| | (1) | (2) | (3) | (4) | (5) | (6) | (7) | (8) | (9) |
| Year | 0.02*** | 0.01 | 0.04*** | 0.00 | 0.04*** | 0.04*** | 0.02** | 0.03*** | 0.00*** |
| | (3.49) | (1.61) | (3.73) | (0.30) | (3.36) | (4.57) | (2.99) | (5.23) | (6.32) |
| Constant | -42.8*** | -22.0 | -73.7*** | -1.87 | -87.2*** | -86.2*** | -35.3** | -66.5*** | -6.96*** |
| | (-3.41) | (-1.53) | (-3.63) | (-0.18) | (-3.31) | (-4.50) | (-2.91) | (-5.08) | (-5.53) |
| $R^2$ | 0.60 | 0.25 | 0.63 | 0.01 | 0.58 | 0.72 | 0.53 | 0.77 | 0.83 |
| F-Value | 12.17 | 2.60 | 13.89 | 0.09 | 11.26 | 20.93 | 8.97 | 27.30 | 39.95 |

**Table S6. Life Table Example.**

Life table format for a given year of $t = 2020$. Columns contains age interval ($x$), central death rate ($m_x$), probability of dying in the age interval ($q_x$), number surviving to exact age ($l_x$), number dying in the interval ($d_x$), person-years lived in the interval ($L_x$), total person-years remaining above age ($T_x$), and life expectancy at exact age ($e_x$).

| $x$ | $m_x$ | $q_x$ | $l_x$ | $d_x$ | $L_x$ | $T_x$ | $e_x$ |
|---|---|---|---|---|---|---|---|
| 0-1 | $m_{0\text{-}1,2020}$ | $q_{0\text{-}1,2020}$ | $l_{0\text{-}1,2020}$ | $d_{0\text{-}1,2020}$ | $L_{0\text{-}1,2020}$ | $T_{0\text{-}1,2020}$ | $e_{0\text{-}1,2020}$ |
| 1-4 | $m_{1\text{-}4,2020}$ | $q_{1\text{-}4,2020}$ | $l_{1\text{-}4,2020}$ | $d_{1\text{-}4,2020}$ | $L_{1\text{-}4,2020}$ | $T_{1\text{-}4,2020}$ | $e_{1\text{-}4,2020}$ |
| 5-9 | $m_{5\text{-}9,2020}$ | $q_{5\text{-}9,2020}$ | $l_{5\text{-}9,2020}$ | $d_{5\text{-}9,2020}$ | $L_{5\text{-}9,2020}$ | $T_{5\text{-}9,2020}$ | $e_{5\text{-}9,2020}$ |
| … | ... | ... | ... | ... | ... | ... | ... |
| 110+ | $m_{110+,2020}$ | $q_{110+,2020}$ | $l_{110+,2020}$ | $d_{110+,2020}$ | $L_{110+,2020}$ | $T_{110+,2020}$ | $e_{110+,2020}$ |

**Table S7. Model fit by teleconnection method.**

This table reports AICc for three teleconnection methods and their paper abbreviations, evaluated on the sample. Lower values indicate a better fit.

| Teleconnection method | Abbreviation | AICc |
|---|---|---|
| Extreme 3-month rolling correlation with E-index (baseline) | Extreme Corr. | -12,957.73 |
| Mean monthly correlation with E-index | Mean Corr. | -12,957.17 |
| Regression coefficient versus E-index | Regressional | -12,946.56 |

## Table S8. E-index Regression Coefficient

This table presents the E-index regression coefficients, applying various fixed effects to ensure robustness against unobserved heterogeneity in the data. Standard errors are clustered at the respective fixed effect level. The displayed values represent the estimated coefficients for each variable, with t-statistics reported in parentheses below. "***" indicates a $p$-value < 0.01, "**" signifies a $p$-value < 0.05, and "*" denotes a $p$-value < 0.1.

| | *Dependent Variable: Mortality Improvement Rate* | | | | | | | |
|---|---|---|---|---|---|---|---|---|
| | (1) | (2) | (3) | (4) | (5) | (6) | (7) | (8) |
| *ENSO measures* | | | | | | | | |
| $E_t$ | 0.29** | 0.38** | 0.28** | 0.38*** | 0.29** | 0.38*** | 0.28** | 0.28** |
| | (2.21) | (2.58) | (2.09) | (2.70) | (2.21) | (2.71) | (2.11) | (2.26) |
| $E_t \times \tau^T$ | -0.07 | -0.04 | -0.05 | 0.00 | -0.07 | -0.02 | -0.07 | -0.05 |
| | (-0.28) | (-0.17) | (-0.21) | (0.01) | (-0.31) | (-0.09) | (0-0.29) | (-0.22) |
| $E_t \times \tau^P$ | -0.26 | -0.21 | -0.26 | -0.18 | -0.28 | -0.21 | -0.27 | -0.25 |
| | (-0.77) | (-0.63) | (-0.77) | (-0.56) | (-0.83) | (-0.67) | (-0.82) | (-0.78) |
| $E_{t-1}$ | 0.31** | 0.44*** | 0.29** | 0.43*** | 0.31** | 0.44*** | 0.28** | 0.29** |
| | (2.47) | (2.93) | (2.48) | (2.89) | (2.50) | (2.91) | (2.40) | (2.37) |
| $E_{t-1} \times \tau^T$ | 0.03 | 0.07 | 0.04 | 0.07 | 0.04 | 0.08 | 0.04 | 0.06 |
| | (0.12) | (0.29) | (0.15) | (0.31) | (0.18) | (0.32) | (0.16) | (0.24) |
| $E_{t-1} \times \tau^P$ | 0.15 | 0.21 | 0.16 | 0.25 | 0.14 | 0.21 | 0.16 | 0.19 |
| | (0.43) | (0.65) | (0.53) | (0.82) | (0.46) | (0.62) | (0.48) | (0.61) |
| $E_{t-2}$ | 0.10 | 0.33* | 0.09 | 0.33* | 0.09 | 0.32 | 0.09 | 0.10 |
| | (0.73) | (1.67) | (0.68) | (1.67) | (0.72) | (1.63) | (0.68) | (0.77) |
| $E_{t-2} \times \tau^T$ | -0.26 | -0.21 | -0.27 | -0.22 | -0.27 | -0.21 | -0.29 | -0.28 |
| | (-0.97) | (-0.78) | (-1.08) | (-0.81) | (-1.09) | (-0.78) | (-1.14) | (-1.11) |
| $E_{t-2} \times \tau^P$ | -0.58* | -0.52 | -0.56*** | -0.49 | -0.59* | -0.53 | -0.59** | -0.57* |
| | (-1.67) | (-1.55) | (-2.68) | (-1.43) | (-1.75) | (-1.58) | (-1.85) | (-1.66) |
| $E_{t-3}$ | 0.35** | 0.60*** | 0.38*** | 0.63*** | 0.36** | 0.61*** | 0.38** | 0.39** |
| | (2.51) | (2.76) | (2.68) | (2.98) | (2.51) | (2.84) | (2.54) | (2.54) |
| $E_{t-3} \times \tau^T$ | 0.23 | 0.28 | 0.21 | 0.25 | 0.23 | 0.29 | 0.21 | 0.22 |
| | (0.79) | (0.99) | (0.74) | (0.91) | (0.81) | (1.04) | (0.76) | (0.83) |
| $E_{t-3} \times \tau^P$ | 1.29*** | 1.36*** | 1.35*** | 1.42*** | 1.31*** | 1.37*** | 1.31*** | 1.39*** |
| | (3.48) | (3.45) | (3.76) | (3.76) | (3.49) | (3.69) | (3.52) | (3.57) |
| $E_{t-4}$ | 0.35** | 0.58*** | 0.36** | 0.59*** | 0.36** | 0.59*** | 0.35** | 0.36** |
| | (2.42) | (2.83) | (2.53) | (3.09) | (2.51) | (2.95) | (2.45) | (2.54) |
| $E_{t-4} \times \tau^T$ | -0.23 | -0.20 | -0.25 | -0.22 | -0.23 | -0.21 | -0.25 | -0.26 |
| | (-0.84) | (-0.75) | (-0.92) | (-0.80) | (-0.84) | (-0.73) | (-0.89) | (-0.94) |
| $E_{t-4} \times \tau^P$ | 0.39 | 0.42 | 0.44 | 0.47 | 0.40 | 0.43 | 0.42 | 0.46 |
| | (0.99) | (1.05) | (1.17) | (1.25) | (1.04) | (1.19) | (1.13) | (1.20) |
| $E_{t-5}$ | 0.33** | 0.38*** | 0.31** | 0.38*** | 0.33*** | 0.39*** | 0.31*** | 0.33** |
| | (2.39) | (2.75) | (2.41) | (2.97) | (2.63) | (2.88) | (2.60) | (2.55) |
| $E_{t-5} \times \tau^T$ | 0.29 | 0.31 | 0.23 | 0.24 | 0.29 | 0.32 | 0.23 | 0.23 |
| | (1.18) | (1.26) | (0.94) | (0.98) | (1.18) | (1.28) | (0.99) | (0.95) |
| $E_{t-5} \times \tau^P$ | 0.55 | 0.55 | 0.54 | 0.56* | 0.56 | 0.56 | 0.52 | 0.57 |
| | (1.49) | (1.56) | (1.63) | (1.67) | (1.64) | (1.64) | (1.58) | (1.62) |
| Control variables | Yes | Yes | Yes | Yes | Yes | Yes | Yes | Yes |
| Country FE | Yes | Yes | No | No | Yes | Yes | No | No |
| Age FE | Yes | Yes | Yes | Yes | No | No | No | No |
| 5-year rolling FE | No | Yes | No | Yes | No | Yes | No | Yes |

## Table S9. Summary Statistics: Mortality Improvement Rates

This table presents the mean mortality improvement rates (in percentages) used in this research, covering 10 countries and regions across 18 age groups. Each cell reports the mean mortality improvement for the corresponding country or region and age group during the sample period, with the standard deviation shown in parentheses below the mean value. The countries and regions included in the analysis are Australia (AUS), Canada (CAN), Chile (CHL), Hong Kong SAR (HKG), Japan (JPN), South Korea (KOR), New Zealand (NZL), Singapore (SGP), Taiwan (TWN), and the United States (USA).

| Age Group | AUS (1) | CAN (2) | CHL (3) | HKG (4) | JPN (5) | NZL (6) | KOR (7) | SGP (8) | TWN (9) | USA (10) |
|---|---|---|---|---|---|---|---|---|---|---|
| 0 | -3.13 | -2.04 | -2.83 | -4.28 | -3.51 | -2.88 | -2.86 | -2.99 | -2.62 | -2.10 |
| | (6.48) | (3.56) | (5.66) | (14.55) | (3.08) | (11.32) | (6.16) | (15.87) | (8.79) | (2.08) |
| 1-4 | -3.79 | -3.02 | -3.19 | -2.03 | -3.96 | -4.13 | -5.45 | -4.39 | -5.18 | -2.46 |
| | (7.98) | (9.42) | (9.65) | (20.11) | (8.88) | (16.15) | (9.50) | (36.38) | (9.57) | (3.24) |
| 5-9 | -4.23 | -3.30 | -4.06 | -2.67 | -3.76 | -3.12 | -7.06 | -2.77 | -4.13 | -2.49 |
| | (8.95) | (9.08) | (10.06) | (29.26) | (13.26) | (24.73) | (12.97) | (13.86) | (14.65) | (5.40) |
| 10-14 | -2.82 | -2.66 | -3.17 | -1.88 | -2.22 | -2.12 | -2.40 | -2.77 | -3.61 | -1.61 |
| | (8.65) | (10.92) | (8.37) | (17.22) | (10.67) | (17.68) | (9.97) | (24.34) | (10.50) | (4.56) |
| 15-19 | -2.50 | -2.39 | -1.28 | -2.07 | -2.11 | -2.40 | -2.58 | -2.77 | -2.53 | -1.14 |
| | (7.93) | (5.70) | (7.07) | (16.73) | (6.74) | (11.11) | (9.33) | (12.80) | (7.47) | (4.85) |
| 20-24 | -2.28 | -1.16 | -1.33 | -2.03 | -1.24 | -2.15 | -2.70 | -3.67 | -2.49 | -0.31 |
| | (5.68) | (5.61) | (5.84) | (14.13) | (4.90) | (10.79) | (5.11) | (19.43) | (5.54) | (4.81) |
| 25-29 | -1.72 | -0.23 | -1.17 | -2.04 | -1.38 | -1.34 | -2.67 | -1.15 | -2.58 | 0.28 |
| | (6.63) | (6.38) | (4.78) | (10.91) | (4.78) | (8.51) | (5.69) | (21.89) | (5.78) | (5.23) |
| 30-34 | -1.08 | -0.03 | -1.18 | -2.50 | -1.51 | -1.73 | -1.62 | -3.39 | -2.32 | 0.69 |
| | (4.20) | (6.33) | (5.29) | (8.14) | (3.79) | (10.59) | (6.12) | (14.32) | (4.50) | (5.57) |
| 35-39 | -1.19 | -0.45 | -0.89 | -2.05 | -1.71 | -1.42 | -2.05 | -2.77 | -1.86 | 0.48 |
| | (4.57) | (5.11) | (3.93) | (6.72) | (3.36) | (7.18) | (3.61) | (12.73) | (3.89) | (5.01) |
| 40-44 | -1.54 | -1.00 | -1.17 | -2.45 | -1.82 | -2.05 | -3.43 | -2.51 | -1.48 | 0.03 |
| | (4.28) | (4.22) | (4.93) | (8.55) | (2.87) | (7.33) | (2.33) | (8.94) | (2.74) | (4.49) |
| 45-49 | -1.86 | -1.48 | -1.13 | -2.21 | -1.96 | -2.09 | -3.54 | -3.07 | -1.45 | -0.41 |
| | (3.33) | (3.37) | (4.46) | (5.39) | (2.38) | (6.92) | (2.28) | (5.19) | (2.55) | (3.56) |
| 50-54 | -2.14 | -1.67 | -1.39 | -2.16 | -1.83 | -2.13 | -3.39 | -2.95 | -1.37 | -0.58 |
| | (2.85) | (2.27) | (4.36) | (6.23) | (2.13) | (5.37) | (1.67) | (6.32) | (2.37) | (3.21) |
| 55-59 | -2.38 | -1.65 | -1.38 | -2.08 | -1.63 | -2.34 | -3.39 | -3.28 | -1.73 | -0.64 |
| | (2.13) | (1.93) | (4.56) | (3.41) | (2.02) | (5.07) | (1.91) | (4.22) | (2.42) | (2.77) |
| 60-64 | -2.40 | -1.68 | -1.07 | -2.61 | -1.69 | -2.42 | -3.45 | -3.40 | -2.07 | -0.69 |
| | (2.50) | (1.96) | (5.00) | (3.83) | (1.94) | (4.42) | (2.03) | (3.71) | (2.16) | (2.97) |
| 65-69 | -2.63 | -1.76 | -1.22 | -2.54 | -1.85 | -2.55 | -4.11 | -3.65 | -2.38 | -0.88 |
| | (2.22) | (1.80) | (4.63) | (3.40) | (1.85) | (2.89) | (1.91) | (3.47) | (2.20) | (2.92) |
| 70-74 | -2.48 | -1.66 | -1.26 | -2.75 | -2.12 | -2.47 | -4.61 | -3.69 | -2.38 | -0.90 |
| | (2.45) | (1.92) | (4.32) | (2.74) | (2.25) | (3.92) | (1.72) | (4.17) | (2.30) | (2.94) |
| 75-79 | -2.26 | -1.50 | -1.21 | -2.16 | -2.35 | -2.09 | -3.56 | -3.26 | -2.09 | -0.65 |
| | (2.69) | (1.49) | (4.61) | (4.15) | (2.18) | (4.00) | (2.63) | (5.76) | (2.59) | (3.11) |
| 80-84 | -1.83 | -1.25 | -1.04 | -2.26 | -2.30 | -1.67 | -2.94 | -2.09 | -1.96 | -0.55 |
| | (3.00) | (1.68) | (5.54) | (5.26) | (2.50) | (3.73) | (2.47) | (3.84) | (3.37) | (3.18) |

## Table S10. Summary Statistics: Economic Controls

This table presents the mean values of the economic control variables used in this research across the 10 countries and regions covered. The variables include GDP per capita, GDP growth, inflation rate, unemployment, interest rate, business and consumer confidence indices, and health expenditure as a percentage of GDP. The standard deviations are reported in parentheses beneath the mean values for each country and region. The countries and regions included in the analysis are Australia (AUS), Canada (CAN), Chile (CHL), Hong Kong SAR (HKG), Japan (JPN), South Korea (KOR), New Zealand (NZL), Singapore (SGP), Taiwan (TWN), and the United States (USA).

| Variables | AUS | CAN | CHL | HKG | JPN | NZL | KOR | SGP | TWN | USA |
|---|---|---|---|---|---|---|---|---|---|---|
| | (1) | (2) | (3) | (4) | (5) | (6) | (7) | (8) | (9) | (10) |
| GDP p.c. ($k.) | 34.73 | 32.00 | 7.95 | 27.06 | 33.31 | 24.50 | 16.70 | 34.03 | 15.60 | 40.11 |
| | (199) | (144) | (53) | (140) | (103) | (139) | (108) | (235) | (85) | (178) |
| GDP Growth | 4.73 | 3.93 | 5.41 | 5.49 | 3.65 | 5.15 | 7.85 | 7.36 | 6.67 | 4.44 |
| | (10.57) | (7.63) | (13.10) | (6.51) | (11.43) | (11.6) | (11.9) | (8.99) | (8.04) | (2.72) |
| Infl. Rate | 3.90 | 3.03 | 9.00 | 4.08 | 0.86 | 4.27 | 4.02 | 1.95 | 1.90 | 3.11 |
| | (2.82) | (2.46) | (8.06) | (4.18) | (1.36) | (4.43) | (3.48) | (2.10) | (2.59) | (1.90) |
| Unempl. Rate | 6.67 | 8.15 | 9.20 | 3.74 | 3.40 | 5.72 | 3.53 | 2.74 | 3.27 | 6.09 |
| | (1.83) | (1.76) | (3.42) | (1.60) | (1.02) | (1.84) | (0.95) | (1.26) | (1.20) | (1.72) |
| Int. Rate | 7.22 | 5.95 | 5.19 | 5.60 | 1.88 | 7.41 | 3.90 | 5.60 | 5.60 | 5.60 |
| | (4.15) | (3.77) | (0.71) | (3.26) | (1.68) | (4.16) | (1.14) | (3.26) | (3.26) | (3.26) |
| Bus. Conf. | 99.96 | 99.95 | 100.03 | 99.92 | 100.03 | 100.02 | 100.00 | 99.92 | 99.92 | 99.80 |
| | (0.94) | (1.16) | (1.73) | (0.96) | (1.33) | (1.58) | (1.46) | (0.96) | (0.96) | (1.03) |
| Cons. Conf. | 99.94 | 100.01 | 99.92 | 100.32 | 99.99 | 99.93 | 99.96 | 100.32 | 100.32 | 100.01 |
| | (1.14) | (1.45) | (1.81) | (1.00) | (1.35) | (1.27) | (0.67) | (1.00) | (1.00) | (1.45) |
| Health/GDP | 7.86 | 9.29 | 7.72 | 7.38 | 7.95 | 7.80 | 4.88 | 7.38 | 7.38 | 13.56 |
| | (1.47) | (1.41) | (0.81) | (0.86) | (1.99) | (1.56) | (1.8) | (0.86) | (0.86) | (2.73) |

## Supplemental Material Reference


86. Dattani, S. *How Does the Risk of Death Change as We Age – and How Has This Changed over Time?* https://ourworldindata.org/how-do-the-risks-of-death-change-as-people-age (2023).

87. Barbi, E., Lagona, F., Marsili, M., Vaupel, J. W. & Wachter, K. W. The plateau of human mortality: Demography of longevity pioneers. *Science* **360**, 1459–1461 (2018).

88. Dickson, D. C., Hardy, M. R. & Waters, H. R. Life table and selection. in *Actuarial mathematics for life contingent risks* 41–70 (Cambridge University Press, 2009).

89. Cashin, P., Mohaddes, K. & Raissi, M. Fair weather or foul? The macroeconomic effects of El Niño. *J. Int. Econ.* **106**, 37–54 (2017).

90. Barro, R. J. Health and economic growth. *Ann. Econ. Financ.* **14**, 329–366 (2013).

91. Kalemli-Ozcan, S. Does the mortality decline promote economic growth? *J. Econ. Growth* **7**, 411–439 (2002).

92. Xing, Y.-F., Xu, Y.-H., Shi, M.-H. & Lian, Y.-X. The impact of PM2.5 on the human respiratory system. *Journal of thoracic disease* **8**, E69 (2016).

93. Hayes, R. B. *et al.* PM2. 5 air pollution and cause-specific cardiovascular disease mortality. *International journal of epidemiology* **49**, 25–35 (2020).

94. Ebi, K. L., Ogden, N. H., Semenza, J. C. & Woodward, A. Detecting and attributing health burdens to climate change. *Environ. Health Perspect.* **125**, 085004 (2017).

95. Ullman, J. B. & Bentler, P. M. Structural equation modeling. *Handbook of psychology, second edition* **2**, (2012).

96. Igolkina, A. A. & Meshcheryakov, G. semopy: A python package for structural equation modeling. *Structural Equation Modeling: A Multidisciplinary Journal* **27**, 952–963 (2020).

97. Callahan, C. W. & Mankin, J. S. Globally unequal effect of extreme heat on economic growth. *Science Advances* **8**, eadd3726 (2022).

98. Gasparrini, A. Distributed lag linear and non-linear models in R: the package dlnm. *Journal of statistical software* **43**, 1–20 (2011).

99. Gasparrini, A., Armstrong, B. & Kenward, M. G. Distributed lag non-linear models. *Statistics in medicine* **29**, 2224–2234 (2010).

100. Chan, D. & Kent, E. SST Data Sets: Overview & Comparison Table. *NSF National Center for Atmospheric Research* https://climatedataguide.ucar.edu/climate-data/sst-data-sets-overview-comparison-table.

101. Gujarati, D. N. & Porter, D. C. *Basic Econometrics*. (McGraw-hill, 2009).

102. Kennedy, P. *A Guide to Econometrics*. (John Wiley & Sons, 2008).

103. Smith, S. C. & Ubilava, D. The El Niño Southern Oscillation and economic growth in the developing world. *Glob. Environ. Chang.* **45**, 151–164 (2017).